

Dioxygen uptake and transfer by Co(III), Rh(III) and Ir(III) catecholate complexes

Pierluigi Barbaro, Claudio Bianchini*, Klaus Linn, Carlo Mealli, Andrea Meli, Francesco Vizza

Istituto per lo Studio della Stereochimica ed Energetica dei Composti di Coordinazione del CNR, 50132 Florence (Italy)

Franco Laschi and Piero Zanello

Dipartimento di Chimica, Università di Siena, 53100 Siena (Italy)

Abstract

A large number of five-coordinate metal catecholate complexes of the general formula $[(\text{triphos})\text{M}(\text{Cat})]\text{Y}$ have been synthesized and characterized by chemical, spectroscopic and electrochemical techniques ($\text{M} = \text{Co}, \text{Rh}, \text{Ir}$; $\text{Cat} = 9,10\text{-phenanthrene catecholate}, 1,2\text{-naphthalene catecholate}, 3,5\text{-di-tert-butylcatecholate}, 4\text{-methylcatecholate}, 4\text{-carboxycatecholate-ethyl ester}, \text{tetrachlorocatecholate}$; $\text{Y} = \text{BPh}_4, \text{PF}_6$; $\text{triphos} = \text{MeC}(\text{CH}_2\text{PPh}_2)_3$). All of the compounds undergo electron-transfer reactions that encompass the $\text{M}(\text{III}), \text{M}(\text{II})$ and $\text{M}(\text{I})$ oxidation states of the metal, and the catecholate, semiquinone and quinone oxidation levels of the quinoid ligand. Paramagnetic $\text{Ir}(\text{III})$ semiquinonate complexes, $[(\text{triphos})\text{Ir}(\text{SQ})]^{2+}$, and $\text{Ir}(\text{II})$ catecholates, $[(\text{triphos})\text{Ir}(\text{Cat})]$, have been characterized by X-band ESR spectroscopy. The reactions of the metal catecholates in non-aqueous media with dioxygen have been investigated. With very few exceptions, all of the compounds react with O_2 to give adducts of the general formula $[(\text{triphos})\text{M}(\text{OO})(\text{SQ})]\text{Y}$. An X-ray analysis has been carried out on $[(\text{triphos})\text{Ir}(\text{OO})(\text{PhenSQ})]\text{BPh}_4$ ($\text{Phen} = 9,10\text{-phenanthrenesemiquinonate}$). In the complex cation, the metal is octahedrally coordinated by the three phosphorus atoms of triphos and by three oxygen atoms, one from O_2 and the other two from the catecholate ligand that has attained a semiquinoid character. The electrochemical behavior of the dioxygen adducts has been studied in detail. Depending on the E° values relative to the $\text{M}^{\text{III}}(\text{SQ})/\text{M}^{\text{III}}(\text{Cat})$ couples of the parent metal catecholates, the dioxygen adducts undergo either a one-electron oxidation to give o -quinone complexes $[(\text{triphos})\text{M}(\text{Q})]^{3+}$ and superoxide ion (O_2^-) or a two-electron oxidation to give $[(\text{triphos})\text{M}(\text{Q})]^{3+}$ and O_2 . Several factors have been found to affect the O_2 uptake by metal catecholates. Of particular importance are: (i) the coordination number of the metal; (ii) the basicity of either the catecholate ligand or metal; (iii) the temperature; (iv) the pressure of dioxygen. The role of each factor has been analyzed and rationalized. The transport of dioxygen from one metal catecholate to another has been studied. A mechanistic interpretation for the formation of the $[(\text{triphos})\text{M}(\text{OO})(\text{SQ})]^+$ complexes is proposed in light of a large crop of experimental data and molecular orbital considerations.

Introduction

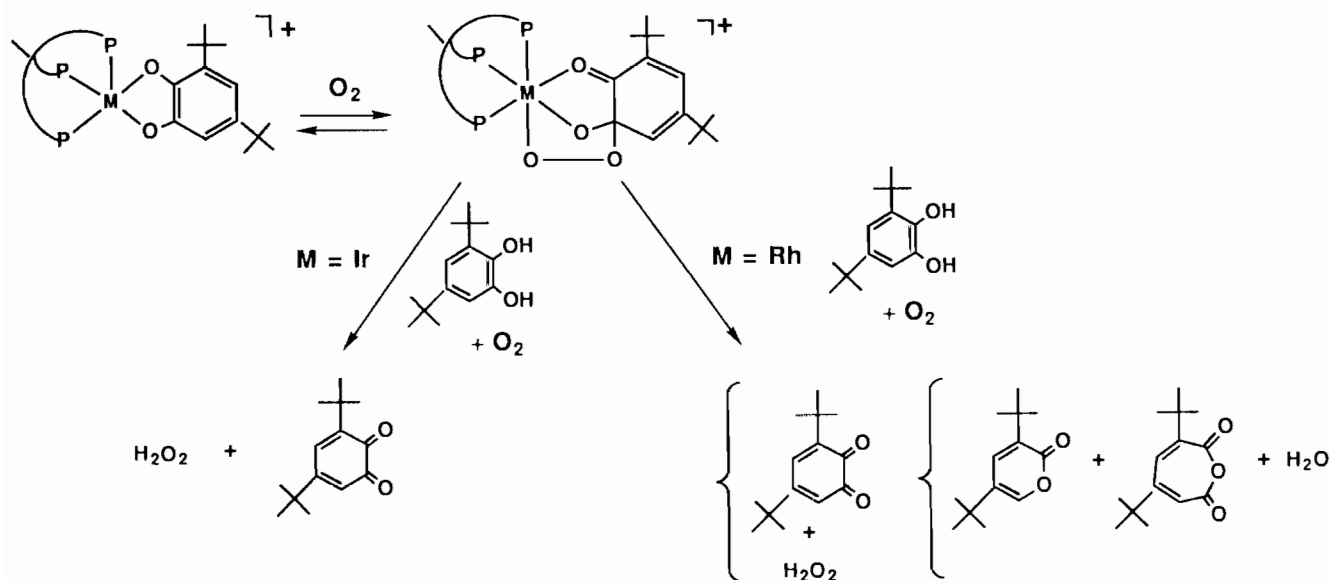
Recently we suggested the use of high-valent transition metal complexes with non-innocent ligands as a method for the activation and transport of molecular oxygen [1–4]. One of the systems we have successfully employed is $[(\text{triphos})\text{M}(\text{DTBC})]^+$ where $\text{M} = \text{Rh}(\text{III})$ [1] or $\text{Ir}(\text{III})$ [4]; $\text{DTBC} = 3,5\text{-di-tert-butylcatecholate}$; $\text{triphos} = \text{MeC}(\text{CH}_2\text{PPh}_2)_3$. These catecholate complexes are able to pick up dioxygen in a reversible manner to give adducts of the type $[(\text{triphos})\text{M}(\text{OO})(\text{SQ})]^+$ ($\text{SQ} = \text{semiquinonate}$), which are homogeneous catalysts for either the oxidation of 3,5-

di-tert-butylcatechol (DTBCH_2) to 3,5-di-tert-butyl-*o*-benzoquinone ($\text{M} = \text{Ir}$ [3, 4], Rh [1]) or the oxygenation of DTBCH_2 to muconic acid anhydride (intradiol C–C cleavage) and 2*H*-pyran-2-one (extradiol C–C cleavage) ($\text{M} = \text{Rh}$) [1, 5] (Scheme 1).

Due to the close relationship of the reactions of Scheme 1 with the activity of certain enzymes, particularly mono- and dioxygenases [5], we decided to carefully investigate the factors that can affect the dioxygen uptake by metal catecholate complexes.

Our study has required the synthesis and characterization of a large number of $[(\text{triphos})\text{M}(\text{Cat})]^+$ complexes where the nature of both the metal and catecholate ligand has been varied as systematically as possible. Also, we have taken into account all of the external factors, including temperature, solvent and

*Author to whom correspondence should be addressed.



Scheme 1.

pressure of dioxygen, that might influence the formation of dioxygen adducts.

We report here the results of our studies, which have shed some light on the interaction between metal catecholate complexes and dioxygen and, hopefully, on the mechanism of activity of catechol dioxygenases.

Experimental

Materials and methods

Abbreviations used: CatH₂ = catechol; DTBCH₂ = 3,5-di-tert-butyl-catechol; PhenH₂ = 9,10-dihydroxyphenanthrene; EDHBH₂ = ethyl-3,4-dihydroxybenzoate; TClCatH₂ = 3,4,5,6-tetrachloro-catechol; 4-MeCatH₂ = 4-methyl-catechol; NaphtH₂ = 1,2-dihydroxynaphthalene; Cat = catecholate; SQ = *o*-semiquinonate; Q = *o*-quinone.

All manipulations were performed under a pure nitrogen atmosphere unless otherwise stated. DTBCH₂, 4-MeCatH₂ and PhenQ were recrystallized from *n*-pentane, *n*-heptane and 1,4-dioxane, respectively. NaphtQ was purified by sublimation. Dichloromethane, dichloroethane, acetone, tetrahydrofuran, *n*-heptane and chloroform were distilled over P₂O₅, Al₂O₃, Na₂CO₃, LiAlH₄, Na and K₂CO₃, respectively. All the other chemicals were commercial products and were used as received without further purification. [(triphos)IrCl(C₂H₄)] [6], [(triphos)RhCl(C₂H₄)] [7], [(triphos)IrCl(O₂)] [8] and [(triphos)Ir(C₂H₄)₂]BPh₄ [6] were prepared according to literature methods. The solid compounds were collected on sintered-glass frits and washed with *n*-pentane before being dried in a stream of nitrogen. IR spectra were recorded on a Perkin-Elmer 1600 Series FT-IR spectrometer using

samples either mullied in Nujol between KBr plates or in CHCl₃ solution; variable-pressure solution spectra were recorded on a Perkin-Elmer 1760 FT-IR spectrometer using a NaCl cell capable of withstanding high pressures (up to 200 atm.). The IR solution experiments were made in a stainless steel vessel (125 ml) having a pressure gauge and two stopcocks. Air was evacuated from the vessel by a vacuum pump, and then a dichloroethane solution of the complex under examination was introduced by suction. The required pressure of oxygen was obtained using a high pressure cylinder. Solution concentration and gas pressures are reported in the presentation of the results. The reaction vessel was connected by a stainless steel capillary coil (total volume 2 ml) to the IR cell. All spectra were recorded after abundant flushing of both coil and IR cell with the solution from the vessel. Proton NMR spectra were recorded at 299.945 MHz on a Varian VXR 300 spectrometer. Chemical shifts are relative to tetramethylsilane as external reference or calibrated against the solvent as the reference signal. ³¹P{¹H} NMR spectra were recorded on a Varian VXR 300 spectrometer operating at 121.42 MHz. Chemical shifts are relative to external 85% H₃PO₄ with downfield values reported as positive. Magnetic susceptibilities of solid samples were measured on a Faraday balance at 21 °C. Conductivities were measured with a model 990101 Orion conductance cell connected to a model 101 conductivity meter. Conductivity data were obtained at sample concentration of *c.* 10⁻³ M at room temperature. UV-Vis spectra were recorded at room temperature on a Shimadzu UV-2100 spectrophotometer using quartz cells. Solutions were about 10⁻⁴ M in CHCl₃. The materials and the apparatus used for electrochemical experiments

have been described elsewhere [1, 2]. Unless otherwise stated, the potential values are relative to an aqueous calomel electrode (SCE) and refer to a controlled temperature (see text). Low-temperature macroelectrolysis tests were performed by using an Ag/AgCl reference electrode, the potential of which was -0.02 V versus SCE. Under the present experimental conditions, the ferrocenium/ferrocene couple was located at $+0.38$ V in acetonitrile solution. X-band ESR spectra were recorded with an ER 200-DSRC Bruker spectrometer operating at $\omega^\circ=9.78$ GHz. The control of the external magnetic field was obtained with a microwave bridge ER 041 MR Bruker wavemeter. The temperature was varied and controlled with an ER 4111 VT Bruker device with an accuracy of $\pm 1^\circ\text{C}$. In order to estimate accurate g_{iso} and g_{aniso} values over the temperature range of interest, the diphenylpicrylhydrazyl free radical (DPPH) was used as field marker (g_{iso} DPPH = 2.0036). In order to ensure quantitative reproducibility, the samples were placed into calibrated quartz capillary tubes permanently positioned in the resonance cavity.

Synthesis of the catecholate complexes

$[(\text{triphos})\text{Ir}(\text{DTBC})]Y$ ($Y = \text{BPh}_4$ (**1a**), PF_6 (**1b**))

Method A. To a solution of $[(\text{triphos})\text{IrCl}(\text{C}_2\text{H}_4)]$ (0.44 g, 0.5 mmol) and DTBQ (0.11 g, 0.5 mmol) in CH_2Cl_2 (20 ml) at room temperature, was added NaBPh_4 (0.21 g, 0.6 mmol) in 15 ml of ethanol. As a result, the orange solution immediately turned violet. On partial evaporation of the solvent, violet crystals of **1a** precipitated in 87% yield. *Anal.* Calc. for $\text{C}_{79}\text{H}_{79}\text{BIrO}_2\text{P}_3$: C, 69.95; H, 5.87; Ir, 14.17; P, 6.85. Found: C, 69.69; H, 5.78; Ir, 14.01; P, 6.74%. The PF_6^- salt **1b** was obtained in 85% yield by using $[\text{Bu}_4\text{N}]\text{PF}_6$ instead of NaBPh_4 . *Anal.* Calc. for $\text{C}_{55}\text{H}_{59}\text{F}_6\text{IrO}_2\text{P}_4$: C, 55.88; H, 5.00; Ir, 16.26; P, 10.50. Found: C, 55.70; H, 5.00; Ir, 16.31; P, 10.47%. $^1\text{H NMR}$ (CDCl_3): δ 1.47 (s, 9H, tert-butyl), 1.49 (s, 9H, tert-butyl).

Method B. A solution of DTBCH₂ (0.06 g, 0.25 mmol) in CH_2Cl_2 (10 ml) was added to $[(\text{triphos})\text{IrCl}(\text{O}_2)]$ (0.22 g, 0.25 mmol) dissolved in 10 ml of CH_2Cl_2 . There was an immediate color change from yellow to violet. After 30 min, NaBPh_4 (0.10 g, 0.3 mmol) in ethanol (30 ml) was added to the mixture. On concentration violet crystals of **1a** were obtained in 80% yield. The reaction produced H_2O_2 in an amount nearly equal to that of the complex obtained, as revealed by iodometry [9].

Method C. An orange mixture of $[(\text{triphos})\text{Ir}(\text{OO})(\text{PhenSQ})]\text{BPh}_4$ (**4a**) (0.69 g, 0.5 mmol) and

DTBCH₂ (1.11 g, 5.0 mmol) was allowed to react in refluxing CH_3NO_2 (8 ml) for 2 h. The color of the solution slowly turned violet. The solution was then cooled to room temperature and 40 ml of n-butanol/n-heptane (1/1) were added causing the separation of violet crystals in 82% yield. The reaction produced H_2O_2 in an amount nearly equal to that of the complex obtained (iodometry).

$[(\text{triphos})\text{Ir}(\text{Phen})]Y$ ($Y = \text{BPh}_4$ (**3a**), PF_6 (**3b**))

Method A. Addition of NaBPh_4 (0.21 g, 0.6 mmol) in ethanol (10 ml) to an orange solution of $[(\text{triphos})\text{IrCl}(\text{C}_2\text{H}_4)]$ (0.44 g, 0.5 mmol) and PhenQ (0.10 g, 0.5 mmol) in CH_2Cl_2 (15 ml) at room temperature gave a deep green solution. On slow evaporation of the solvent green-blue crystals of **3a** precipitated in 85% yield. *Anal.* Calc. for $\text{C}_{79}\text{H}_{67}\text{BIrO}_2\text{P}_3$: C, 70.58; H, 5.02; Ir, 14.29; P, 6.91. Found: C, 70.11; H, 4.98; Ir, 14.01; P, 6.77%. Compound **3b** was prepared using $[\text{Bu}_4\text{N}]\text{PF}_6$ instead of NaBPh_4 . *Anal.* Calc. for $\text{C}_{55}\text{H}_{47}\text{F}_6\text{IrO}_2\text{P}_4$: C, 56.45; H, 4.02; Ir, 16.44; P, 10.61. Found: C, 56.55; H, 4.00; Ir, 16.24; P, 10.48%. $^1\text{H NMR}$ (CDCl_3): δ 7.52 (m, 2H, H_2+H_3), 7.98 (dd, 1H, H_4), 8.38 (dd, 1H, H_1), $J(\text{H}_1\text{H}_2)=7.8$, $J(\text{H}_1\text{H}_3)=0.02$, $J(\text{H}_2\text{H}_3)=7.87$, $J(\text{H}_2\text{H}_4)=0.67$, $J(\text{H}_3\text{H}_4)=7.31$ Hz.

Method B. PhenQ (0.08 g, 0.39 mmol) was added to $[(\text{triphos})\text{Ir}(\text{C}_2\text{H}_4)_2]\text{BPh}_4$ (0.45 g, 0.39 mmol) dissolved in CH_2Cl_2 (15 ml). Addition of ethanol and slow evaporation of the solvent under a stream of nitrogen gave blue crystals of **3a** in 85% yield.

$[(\text{triphos})\text{Ir}(4\text{-MeCat})]\text{BPh}_4$ (**5**)

Method A. A mixture of $[(\text{triphos})\text{Ir}(\text{OO})(\text{PhenSQ})]\text{BPh}_4$ (**4a**) (0.55 g, 0.4 mmol) and 4-MeCatH₂ (0.50 g, 4.0 mmol) was stirred in refluxing CH_3NO_2 (8 ml) for 2 h. The color of the solution slowly turned purple. The solution was then cooled to room temperature and 40 ml of n-butanol/n-heptane (1/1) were added causing the separation of purple-red crystals in 70% yield. *Anal.* Calc. for $\text{C}_{72}\text{H}_{65}\text{BIrO}_2\text{P}_3$: C, 68.74; H, 5.17; Ir, 15.29; P, 7.40. Found: C, 68.66; H, 5.12; Ir, 15.17; P, 7.54%. $^1\text{H NMR}$ (CDCl_3): δ 2.50 (s, 3H, CH_3). The reaction produced H_2O_2 in an amount nearly equal to that of the complex obtained (iodometry).

Method B. A solution of 4-MeCatH₂ (0.085 g, 0.68 mmol) in CH_2Cl_2 (10 ml) was added to $[(\text{triphos})\text{IrCl}(\text{O}_2)]$ (0.60 g, 0.68 mmol) dissolved in 10 ml of CH_2Cl_2 . There was an immediate color change from yellow to purple. After 30 min NaBPh_4 (0.24 g, 0.70 mmol) in ethanol (30 ml) was added to the mixture. On concentration purple-red crystals were obtained in

75% yield. In the reaction H_2O_2 was produced in an amount nearly equal to that of the complex obtained (iodometry). We were not able to prepare the PF_6^- salt of this compound due to decomposition of the complex in solution.

[(triphos)Ir(Napht)]Y ($Y = \text{BPh}_4$ (7a), PF_6 (7b))

Method A. A solution of NaphtQ (0.054 g, 0.34 mmol) in CH_2Cl_2 (10 ml) was added to [(triphos)IrCl(C_2H_4)] (0.30 g, 0.34 mmol) dissolved in CH_2Cl_2 (10 ml). After 10 min, a solution of NaBPh_4 (0.17 g, 0.34 mmol) in ethanol (20 ml) was added causing the reaction mixture to change its color from red to blue-green. On evaporation of the solvent in a stream of nitrogen, blue crystals were obtained in 77% yield. *Anal.* Calc. for $\text{C}_{75}\text{H}_{65}\text{BIrO}_2\text{P}_3$: C, 69.60; H, 5.03; Ir, 14.85; P, 7.19. Found: C, 69.47; H, 4.98; Ir, 14.77; P, 7.24%. The PF_6^- salt **7b** was obtained in 73% yield by using $[\text{Bu}_4\text{N}]\text{PF}_6$ instead of NaBPh_4 . *Anal.* Calc. for $\text{C}_{51}\text{H}_{45}\text{F}_6\text{IrO}_2\text{P}_4$: C, 54.68; H, 4.02; Ir, 17.17; P, 11.08. Found: C, 54.50; H, 4.07; Ir, 17.06; P, 11.27. ^1H NMR (CDCl_3): δ 6.45 (d, 1H, $J(\text{HH}) = 10.86$ Hz), 7.62 (td, 1H, $J(\text{HH}) = 7.84$, 1.3 Hz), 8.12 (dd, 1H, $J(\text{HH}) = 8.04$, 1.5 Hz). Other resonances of catecholate protons are masked by those of the phenyl system of triphos.

Method B. NaphtQ (0.08 g, 0.50 mmol) was added to [(triphos)Ir(C_2H_4) $_2$]BPh $_4$ (0.58 g, 0.50 mmol) dissolved in CH_2Cl_2 (15 ml). The solution was evaporated to dryness under vacuum and the resulting blue solid washed with n-pentane and dried under vacuum.

[(triphos)IrCl(TClCat)] (9)

A solution of TClQ (0.11 g, 0.45 mmol) in CH_2Cl_2 (10 ml) was added to a solution of [(triphos)IrCl(C_2H_4)] (0.40 g, 0.45 mmol) in CH_2Cl_2 (10 ml). On standing, yellow crystals of **9** slowly separated in 83% yield. *Anal.* Calc. for $\text{C}_{47}\text{H}_{39}\text{Cl}_2\text{IrP}_3\text{O}_2$: C, 51.39; H, 3.55; Ir, 17.51; P, 8.47. Found: C, 51.02; H, 3.45; Ir, 17.77; P, 8.54%.

[(triphos)IrCl(TClCat)]PF $_6$ (10)

A mixture of [(triphos)IrCl(TClCat)] (**9**) (0.30 g, 0.27 mmol) and TlPF $_6$ (0.11 g, 0.30 mmol) in acetone (20 ml) was heated at reflux temperature. After 2 h, the red solution obtained was cooled down to room temperature and the TlCl residue filtered off. On addition of n-heptane, a red solid precipitated in 89% yield. *Anal.* Calc. for $\text{C}_{47}\text{H}_{39}\text{Cl}_4\text{F}_6\text{IrP}_4\text{O}_2$: C, 46.73; H, 3.23; Ir, 15.93; P, 10.27. Found: C, 46.88; H, 3.24; Ir, 15.88; P, 10.54%.

[(triphos)IrCl(EDHB)] (11)

A solution of [(triphos)IrCl(O_2)] (0.60 g, 0.68 mmol) in CH_2Cl_2 (10 ml) was added to a suspension of EDHBH $_2$

(0.13 g, 0.70 mmol) in CH_2Cl_2 (20 ml). The yellow solution immediately turned deep orange. After filtering off the undissolved EDHBH $_2$, ethanol was added to the filtrate causing the precipitation of yellow crystals in 75% yield. *Anal.* Calc. for $\text{C}_{50}\text{H}_{47}\text{ClIrP}_3\text{O}_4$: C, 58.16; H, 4.56; Ir, 18.63; P, 9.01. Found: C, 58.02; H, 4.54; Ir, 18.35; P, 9.12%. ^1H NMR (CDCl_3): δ 1.33 (t, 3H, $\text{CO}_2\text{CH}_2\text{CH}_3$), 4.28 (q, 2H, $\text{CO}_2\text{CH}_2\text{CH}_3$), $J(\text{HH}) = 4.10$ Hz. The reaction produced H_2O_2 in an amount nearly equal to that of the complex obtained (iodometry).

[(triphos)Ir(EDHB)]Y ($Y = \text{BPh}_4$ (12a), PF_6 (12b))

Method A. A mixture of [(triphos)Ir($\overline{\text{OO}}$)(PhenSQ)]BPh $_4$ (**4a**) (0.50 g, 0.36 mmol) and EDHBH $_2$ (0.65 g, 3.6 mmol) was stirred in refluxing CH_3NO_2 (8 ml) for 2 h. The color of the solution slowly turned from orange to violet. After cooling down to room temperature, 30 ml of n-butanol were added causing the separation of purple crystals in 80% yield. *Anal.* Calc. for $\text{C}_{74}\text{H}_{67}\text{BIrO}_4\text{P}_3$: C, 67.53; H, 5.10; Ir, 14.62; P, 7.07. Found: C, 67.82; H, 5.12; Ir, 14.27; P, 7.34%. Compound **12b** was obtained using **4b** instead of **4a**. *Anal.* Calc. for $\text{C}_{50}\text{H}_{47}\text{F}_6\text{IrO}_4\text{P}_4$: C, 52.58; H, 4.12; Ir, 16.84; P, 10.87. Found: C, 52.68; H, 4.07; Ir, 17.02; P, 10.57%. ^1H NMR (CDCl_3): δ 1.46 (t, 3H, $\text{CO}_2\text{CH}_2\text{CH}_3$), 4.22 (q, 2H, $\text{CO}_2\text{CH}_2\text{CH}_3$), $J(\text{HH}) = 7.15$ Hz. The reactions produced H_2O_2 in an amount nearly equal to that of the complex obtained (iodometry).

Method B. A mixture of [(triphos)IrCl(EDHB)] (**11**) (0.31 g, 0.30 mmol) and TlPF $_6$ (0.11 g, 0.30 mmol) dissolved in acetone (20 ml) was heated at 40 °C for 1 h. The resulting purple solution was cooled to room temperature and the TlCl residue was filtered off. On addition of n-heptane purple crystals precipitated in 80% yield.

[(triphos)Rh(DTBC)]Y ($Y = \text{BPh}_4$ (14a), PF_6 (14b))

Method A. DTBQ (0.22 g, 1 mmol) in CH_2Cl_2 (10 ml) was added to a CH_2Cl_2 (30 ml) solution of [(triphos)RhCl(C_2H_4)] (0.79 g, 1 mmol). There was an immediate color change from orange to deep green. After 10 min, NaBPh_4 (0.34 g, 1 mmol) in ethanol (30 ml) was added, and the resulting solution was slowly concentrated in a stream of nitrogen to give green crystals in 85% yield. *Anal.* Calc. for $\text{C}_{79}\text{H}_{79}\text{BO}_2\text{P}_3\text{Rh}$: C, 76.88; H, 6.28; P, 7.54; Rh, 8.12. Found: C, 76.24; H, 6.15; P, 7.77; Rh, 7.96%. Compound **14b** was obtained by using $[\text{n-Bu}_4\text{N}]\text{PF}_6$ instead of NaBPh_4 . *Anal.* Calc. for $\text{C}_{55}\text{H}_{59}\text{F}_6\text{O}_2\text{P}_4\text{Rh}$: C, 60.44; H, 5.40; P, 11.36; Rh, 9.43. Found: C, 60.65; H, 5.55; P, 11.20; Rh 9.67%. ^1H NMR (CDCl_3): δ 1.43 (s, 9H, tert-butyl), 1.46 (s, 9H, tert-butyl).

Method B. A mixture of $[(\text{triphos})\overline{\text{Rh}}(\overline{\text{O}}\overline{\text{O}})(\overline{\text{PhenSQ}})]\text{BPh}_4$ (**17a**) (0.39 g, 0.30 mmol) and DTBCH₂ (0.67 g, 3.0 mmol) was stirred for 4 h in CH₂Cl₂ solution (20 ml) at room temperature. The yellow solution slowly turned green. Addition of n-butanol (10 ml) and slow evaporation of the solvent in a stream of nitrogen caused the separation of green crystals in 78% yield. H₂O₂ was produced in an amount nearly equal to that of the complex obtained (iodometry).

$[(\text{triphos})\text{Rh}(\text{Phen})]\text{Y}$ ($\text{Y}=\text{BPh}_4$ (**16a**), PF₆ (**16b**))

To a solution of $[(\text{triphos})\text{RhCl}(\text{C}_2\text{H}_4)]$ (0.40 g, 0.5 mmol) and PhenQ (0.10 g, 0.50 mmol) in CH₂Cl₂ (20 ml) at room temperature was added NaBPh₄ (0.21 g, 0.6 mmol) in 15 ml of ethanol. Upon addition of NaBPh₄, the orange solution turned green. On partial evaporation of the solvent under a stream of nitrogen, green crystals precipitated. They were filtered off, washed and dried. Yield 83%. *Anal.* Calc. for C₇₉H₆₇BO₂P₃Rh: C, 75.61; H, 5.34; P, 7.42; Rh, 8.22. Found: C, 75.77; H, 5.45; P, 7.14; Rh, 8.01%. The PF₆⁻ salt **16b** was obtained in 85% yield by using [Bu₄N]PF₆ instead of NaBPh₄. *Anal.* Calc. for C₅₅H₄₇F₆O₂P₄Rh: C, 61.11; H, 4.35; P, 11.48; Rh, 9.54. Found: C, 61.27; H, 4.40; P, 11.22; Rh 9.32%. ¹H NMR (CDCl₃): δ 7.68 (m, 2H, H₂+H₃), 8.42 (dd, 1H, H₄), 8.67 (dd, 1H, H₁), J(H₁H₂)=7.1, J(H₁H₃)=0.10, J(H₂H₃)=7.75, J(H₂H₄)=0.58, J(H₃H₄)=7.30 Hz.

$[(\text{triphos})\text{Rh}(\text{EDHB})]\text{Y}$ ($\text{Y}=\text{BPh}_4$ (**18a**), PF₆ (**18b**))

Method A. A mixture of $[(\text{triphos})\overline{\text{Rh}}(\overline{\text{O}}\overline{\text{O}})(\overline{\text{PhenSQ}})]\text{BPh}_4$ (**17a**) (0.39 g, 0.30 mmol) and EDHBH₂ (0.54 g, 3.0 mmol) in CHCl₃ (20 ml) was stirred for 30 min at 50 °C. The color of the solution slowly changed from yellow to green–blue. After cooling down to room temperature and filtering off the unreacted EDHBH₂, n-butanol (20 ml) was added. Slow evaporation of the solvent in a stream of nitrogen gave blue crystals in 80% yield. *Anal.* Calc. for C₇₄H₆₇BO₄P₃Rh: C, 72.44; H, 5.46; P, 7.59; Rh, 8.40. Found: C, 72.67; H, 5.55; P, 7.76; Rh, 8.26%. Compound **18b** was obtained using **17b** instead of **17a**. *Anal.* Calc. for C₅₀H₄₇F₆O₄P₄Rh: C, 57.03; H, 4.47; P, 11.79; Rh, 9.79. Found: C, 57.30; H, 4.45; P, 11.52; Rh 9.54%. ¹H NMR (CDCl₃): δ 1.45 (t, 3H, CO₂CH₂CH₃), 4.43 (q, 2H, CO₂CH₂CH₃), J(HH)=7.10 Hz. In the reaction H₂O₂ was produced in an amount nearly equal to that of the complex obtained, as revealed by iodometry.

Method B. A mixture of $[(\text{triphos})\text{Rh}(\text{DTBC})]\text{BPh}_4$ (**14a**) (0.62 g, 0.50 mmol) and EDHBH₂ (0.90 g, 5.0 mmol) in CH₂Cl₂ (20 ml) under oxygen was allowed to react overnight at -16 °C to give a green–blue solution. After heating to room temperature, n-butanol

(10 ml) was added. Slow evaporation of the solvent in a stream of nitrogen gave blue crystals in 76% yield.

$[(\text{triphos})\text{Rh}(\text{Napht})]\text{Y}$ ($\text{Y}=\text{BPh}_4$ (**19a**), PF₆ (**19b**))

To a solution of $[(\text{triphos})\text{RhCl}(\text{C}_2\text{H}_4)]$ (0.27 g, 0.3 mmol) and NaphtQ (0.05 g, 0.30 mmol) in CH₂Cl₂ (20 ml) at room temperature was added NaBPh₄ (0.34 g, 0.4 mmol) in 15 ml of ethanol. Upon addition of NaBPh₄, the orange solution turned green. On partial evaporation of the solvent under a stream of nitrogen, green crystals precipitated in 88% yield. *Anal.* Calc. for C₇₅H₆₅BO₂P₃Rh: C, 74.76; H, 5.40; P, 7.72; Rh, 8.56. Found: C, 74.67; H, 5.45; P, 7.14; Rh, 8.26%. The PF₆ derivative **19b** was obtained in 80% yield by using [Bu₄N]PF₆ instead of NaBPh₄. *Anal.* Calc. for C₅₁H₄₅F₆O₂P₄Rh: C, 59.42; H, 4.37; P, 12.04; Rh, 10.00. Found: C, 59.32; H, 4.28; P, 12.32; Rh 9.76%. ¹H NMR (CDCl₃): δ 6.35 (d, 1 H, J(HH)=10.33 Hz), 7.97 (dd, 1H, J(HH)=8.16, 1.3 Hz). Other resonances of catecholate protons are masked by those of the phenyl system of triphos.

$[(\text{triphos})\text{Rh}(4\text{-MeCat})]\text{Y}$ ($\text{Y}=\text{BPh}_4$ (**21a**), PF₆ (**21b**))

A mixture of $[(\text{triphos})\overline{\text{Rh}}(\overline{\text{O}}\overline{\text{O}})(\overline{\text{PhenSQ}})]\text{BPh}_4$ (**17a**) (0.39 g, 0.30 mmol) and 4-MeCatH₂ (0.37 g, 3.0 mmol) was stirred for 1 h at 50 °C in CHCl₃ solution (20 ml). The color of the parent yellow solution slowly turned green. The solution was cooled to room temperature and n-butanol (20 ml) was added. Slow evaporation of the solvent in a stream of nitrogen caused the separation of green crystals in 80% yield. *Anal.* Calc. for C₇₂H₆₅BO₂P₃Rh: C, 73.98; H, 5.57; P, 7.96; Rh, 8.82. Found: C, 73.54; H, 5.45; P, 7.76; Rh, 8.96%. Compound **21b** was obtained in 76% yield by using **17b** instead of **17a**. *Anal.* Calc. for C₄₈H₄₅F₆O₂P₄Rh: C, 57.95; H, 4.53; P, 12.47; Rh, 10.36. Found: C, 57.86; H, 4.58; P, 12.76; Rh 10.30%. ¹H NMR (CDCl₃): δ 2.43 (s, 3H, CH₃). H₂O₂ was produced in an amount nearly equal to that of the complex obtained (iodometry).

$[(\text{triphos})\text{Co}(\text{DTBC})]\text{ClO}_4$ (**23**)

A solution of Co(ClO₄)₂·6H₂O (0.36 g, 1 mmol) in n-butanol (100 ml) was carefully concentrated at reflux temperature to c. 5 ml. Triphos (0.62 g, 1 mmol) in CH₂Cl₂ (10 ml) was then added, followed by DTBQ (0.22 g, 1 mmol) in CH₂Cl₂ (10 ml). A rapid color change of the solution from orange to blue was observed. Addition of di-n-butyl ether (30 ml) caused the precipitation of green–blue crystals in 73% yield. *Anal.* Calc. for C₅₅H₅₉ClCoO₆P₃: C, 65.85; H, 5.93; Co, 5.87. Found: C, 65.71; H, 5.85; Co, 5.79%. ¹H NMR (CDCl₃): δ 1.37 (s, 9H, tert-butyl), 1.42 (s, 9H, tert-butyl).

Caution. To avoid detonation of Co(ClO₄)₂, the solution must not be taken to near dryness nor should

solid material be allowed to deposit on the walls of the reaction flask. It is recommended to work behind a protective barrier.

[(triphos)Co(Phen)]ClO₄ (24)

A solution of Co(ClO₄)₂·6H₂O (0.36 g, 1 mmol) in n-butanol (100 ml) was carefully concentrated at reflux temperature to c. 5 ml. Triphos (0.62 g, 1 mmol) in CH₂Cl₂ (10 ml) was then added followed by PhenQ (0.21 g, 1 mmol) in CH₂Cl₂ (10 ml). A rapid color change of the solution from orange to blue was observed. Addition of di-n-butyl ether (30 ml) caused the precipitation of green crystals in 80% yield. *Anal.* Calc. for C₅₅H₄₇ClCoO₆P₃: C, 66.63; H, 4.74; Co, 5.96; P, 9.39. Found: C, 65.87; H, 4.56; Co, 6.12; P, 9.50%. No precise ¹H NMR (CDCl₃) assignment of the protons of Phen can be made as these resonances are obscured by those of the phenyl system of triphos.

[(triphos)Co(Napht)]ClO₄ (26)

A solution of Co(ClO₄)₂·6H₂O (0.36 g, 1 mmol) in n-butanol (100 ml) was carefully concentrated at reflux temperature to c. 5 ml. Triphos (0.62 g, 1 mmol) in CH₂Cl₂ (10 ml) was then added followed by NaphtQ (0.16 g, 1 mmol) in CH₂Cl₂ (10 ml). A rapid color change of the solution from orange to blue was observed. Addition of di-n-butyl ether (30 ml) caused the precipitation of green-blue crystals in 78% yield. *Anal.* Calc. for C₅₁H₄₅ClCoO₆P₃: C, 65.08; H, 4.78; Co, 6.26; P, 9.89. Found: C, 64.87; H, 4.59; Co, 6.20; P, 9.70%. No precise ¹H NMR (CDCl₃) assignment of the protons of Napht can be made as these resonances are obscured by those of the phenyl system of triphos.

Synthesis of the oxygenated complexes

Most of the complexes of the general formula [(triphos)M(OO)(SQ)]Y, were isolated in the solid state by bubbling O₂ throughout a CH₂Cl₂ solution of the corresponding catechol derivative at the appropriate temperature. Crystals were obtained by addition of n-butanol. Only ¹H NMR data are reported for the dioxygen adducts prepared in solution (see Table 8 for ³¹P{¹H} NMR).

[(triphos)Ir(OO)(DTBSQ)]Y (Y=BPh₄ (2a), PF₆ (2b))

Anal. Calc. for C₇₉H₇₉BIrO₄P₃ (2a): C, 68.33; H, 5.74; Ir, 13.85; P, 6.70. Found: C, 68.54; H, 5.78; Ir, 13.74; P, 6.57%. *Anal.* Calc. for C₅₅H₅₉F₆IrO₄P₄ (2b): C, 54.40; H, 4.86; Ir, 15.84; P, 10.22. Found: C, 54.56; H, 4.75; Ir, 15.67; P, 10.20%. ¹H NMR (CDCl₃): δ 1.34 (s, 9H, tert-butyl), 1.37 (s, 9H, tert-butyl).

[(triphos)Ir(OO)(PhenSQ)]Y·0.5CH₂Cl₂ (Y=BPh₄ (4a), PF₆ (4b))

Anal. Calc. for C_{79.5}H₆₈BClIrO₄P₃ (4a): C, 67.30; H, 4.83; Ir, 13.55; P, 6.55. Found: C, 67.15; H, 4.78; Ir, 13.41; P, 6.37%. *Anal.* Calc. for C_{55.5}H₄₈ClF₆IrO₄P₄ (4b): C, 54.33; H, 3.92; Ir, 15.66; P, 10.12. Found: C, 54.66; H, 3.95; Ir, 15.89; P, 10.11%. ¹H NMR (CDCl₃): δ 7.52 (td, 1H, H₃), 7.74 (td, 1H, H₂), 7.98 (dd, 1H, H₄), 8.10 (dd, 1H, H₁), J(H₁H₂)=7.90, J(H₁H₃)=-0.04, J(H₂H₃)=7.36, J(H₂H₄)=0.64, J(H₃H₄)=7.99 Hz.

[(triphos)Ir(OO)(4-MeSQ)]BPh₄ (6)

Dioxygen was bubbled through a solution of **5** in CH₂Cl₂ cooled to -78 °C (dry-ice/acetone bath) for 30 min. Precooled n-heptane was then added until the separation of an orange solid occurred. The solid was filtered off, washed with n-pentane and dried under vacuum. *Anal.* Calc. for C₇₂H₆₅BIrO₄P₃: C, 67.03; H, 5.04; Ir, 14.91; P, 7.21. Found: C, 69.94; H, 5.00; Ir, 14.92; P, 7.19%. ¹H NMR (CDCl₃, -50 °C): δ 2.35 (s, 3H, CH₃).

[(triphos)Ir(OO)(NaphtSQ)]Y (Y=BPh₄ (8a), PF₆ (8b))

Anal. Calc. for C₇₅H₆₅BIrO₄P₃ (8a): C, 67.92; H, 4.91; Ir, 14.51; P, 7.02. Found: C, 67.65; H, 4.84; Ir, 14.44; P, 7.22%. *Anal.* Calc. for C₅₁H₄₅F₆IrO₄P₄ (8b): C, 53.16; H, 3.91; Ir, 16.70; P, 10.77. Found: C, 53.27; H, 4.05; Ir, 16.82; P, 10.51%. ¹H NMR (CDCl₃): δ 6.40 (d, 1H, J(HH)=11.00 Hz), 7.55 (td, 1H, J(HH)=7.25, 1.3 Hz), 7.70 (td, 1H, J(HH)=7.56, 1.5 Hz), 7.93 (d, 1H, J(HH)=9.64 Hz). Other resonances of catecholate protons are masked by those of the phenyl system of triphos.

[(triphos)Ir(OO)(EDHBSQ)]Y (Y=BPh₄ (13a), PF₆ (13b))

¹H NMR (CD₂Cl₂, -90 °C): δ 1.36 (t, 3H, CO₂CH₂CH₃), 4.30 (q, 2H, CO₂CH₂CH₃), J(HH)=7.10 Hz.

[(triphos)Rh(OO)(DTBSQ)]Y (Y=BPh₄ (15a), PF₆ (15b))

¹H NMR CDCl₃, -20 °C): δ 1.20 (s, 9H, tert-butyl), 1.22 (s, 9H, tert-butyl).

[(triphos)Rh(OO)(PhenSQ)]Y (Y=BPh₄ (17a), PF₆ (17b))

Anal. Calc. for C₇₉H₆₇BO₄P₃Rh (17a): C, 73.73; H, 5.21; P, 7.23; Rh, 8.01. Found: C, 74.00; H, 5.28; P, 7.37; Rh, 7.95%. *Anal.* Calc. for C₅₅H₄₇F₆O₄P₄Rh (17b): C, 59.35; H, 4.23; P, 11.15; Rh, 9.26. Found: C, 59.45; H, 4.28; P, 11.36; Rh, 9.02%. ¹H NMR (CDCl₃): δ 7.50 (dd, 1H, H₃), 7.73 (dd, 1H, H₂), 7.97 (d, 1H, H₄), 8.08

(d, 1H, H_1), $J(H_1H_2)=8.03$, $J(H_2H_3)=7.31$, $J(H_3H_4)=7.80$ Hz.

[(triphos)Rh(OO)(NaphtSQ)]Y ($Y=BPh_4$ (20a), PF_6 (20b))

Anal. Calc. for $C_{75}H_{65}BO_4P_3Rh$ (20a): C, 72.83; H, 5.26; P, 7.52; Rh, 8.33. Found: C, 73.01; H, 5.18; P, 7.40; Rh, 7.96%. *Anal.* Calc. for $C_{51}H_{45}F_6O_4P_4Rh$ (20b): C, 57.63; H, 4.24; P, 11.68; Rh, 9.70. Found: C, 57.58; H, 4.30; P, 11.45; Rh, 9.40%. 1H NMR ($CDCl_3$): δ 6.41 (d, 1H, $J(HH)=10.06$ Hz), 8.06 (dd, 1H, $J(HH)=7.98$, 1.5 Hz). Other resonances of catecholate protons are masked by those of the phenyl system of triphos.

[(triphos)Rh(OO)(4-MeSQ)]Y ($Y=BPh_4$ (22a), PF_6 (22b))

1H NMR ($CDCl_3$, -50 °C): δ 2.28 (s, 3H, CH_3).

No precise 1H NMR assignments of semiquinonate protons of [(triphos)Co(OO)(PhenSQ)]ClO₄ (25) and [(triphos)Co(OO)(NaphtSQ)]ClO₄ (27) can be made as these resonances are obscured by those of the phenyl system of triphos.

Dioxygen transfer between metal catecholate complexes

Dioxygen transfer reactions between catecholate complexes were performed by stirring for 30 min equimolar amounts of a dioxygen adduct, stable in the experimental conditions (deaerated solution at 20 °C), and of a metal catecholate complex in an appropriate solvent. The product composition of the resulting solution was analyzed by $^{31}P\{^1H\}$ NMR spectroscopy.

Reaction 1. 30 mg of [(triphos)Rh(OO)(PhenSQ)]- BPh_4 (0.02 mmol) and 27 mg of [(triphos)Ir(Phen)] BPh_4 (0.02 mmol) were dissolved in CD_3NO_2 (3 ml). ^{31}P NMR analysis gave: [(triphos)Rh(OO)(PhenSQ)]- $BPh_4 \rightleftharpoons$ [(triphos)Ir(Phen)] $BPh_4 \rightleftharpoons 43\%$; [(triphos)Rh(Phen)] $BPh_4 \rightleftharpoons$ [(triphos)Ir(OO)(PhenSQ)] $BPh_4 \rightleftharpoons 57\%$.

Reaction 2. 30 mg of [(triphos)Ir(OO)(NaphtSQ)]- BPh_4 (0.02 mmol) and 25 mg of [(triphos)Rh(Phen)] BPh_4 (0.02 mmol) were dissolved in $CDCl_3$ (3 ml). ^{31}P NMR analysis gave: [(triphos)Ir(OO)(NaphtSQ)] $BPh_4 \rightleftharpoons$ [(triphos)Rh(Phen)] $BPh_4 \rightleftharpoons 65\%$; [(triphos)Ir(Napht)] $BPh_4 \rightleftharpoons$ [(triphos)Rh(OO)(PhenSQ)] $BPh_4 \rightleftharpoons 35\%$.

X-ray data collection and structure determination

Crystal and intensity data are reported in Table 1. X-ray measurements were performed on Enraf-Nonius CAD4 diffractometer. The cell constants and orientation matrix were determined by least-squares refinement of the setting angles for 25 reflections. The intensities of three standard reflections were measured every 120 min of X-ray exposure (Mo $K\alpha$). An overall decay of c. 10% was observed. Due to this behavior, the data were corrected on the basis of these standards. The

TABLE 1. Summary of crystal data for [(triphos)Ir(OO)(PhenSQ)] $BPh_4 \cdot 0.5CH_2Cl_2$

Formula	$C_{79.5}H_{68}BClIrO_4P_3$
Molecular weight	1418.71
Crystal system	triclinic
Space group	$P1$
a (Å)	10.794(4)
b (Å)	16.679(5)
c (Å)	19.586(3)
α (°)	84.94(2)
β (°)	76.79(2)
γ (°)	78.93(2)
V (Å ³)	3383.48
Z	2
D_{calc} (g cm ⁻³)	1.43
μ (Mo $K\alpha$) (cm ⁻¹)	21.2
Radiation	graphite-monochromated Mo $K\alpha$, $\lambda=0.71069$ Å
Scan type	ω -2 θ
2 θ range (°)	5–45
Scan width (°)	$1.0+0.35(\tan \theta)$
Scan speed (° min ⁻¹)	8.23
Total no. data	9495
No. unique data with $I > 3\sigma(I)$	5548
No. parameters	355
R	0.065
R_w	0.065
Absorption correction:	0.6, 0.9
min., max.	

data were also corrected for Lorentz and polarization effects. An empirical correction for the absorption effect was made by using the program DIFABS [10]. Atomic scattering factors were those tabulated by Cromer and Waber [11] with anomalous dispersion correction taken from ref. 12. The computation work was essentially performed by using the SHELX76 system [13]. The structure was solved by a combination of Patterson and direct-method techniques. A series of F_o Fourier syntheses allowed the location of all the non-hydrogen atoms. During the least-squares refinements the phenyl rings were treated as rigid bodies (D_{6h} symmetry) with the C–C distances fixed at 1.39 Å. Anisotropic thermal parameters were used for Ir, P and O atoms. The hydrogen atoms were included at calculated positions (C–H=1.08 Å). After a final least-squares cycle ($R=0.065$, $R_w=0.065$) a ΔF map appeared essentially featureless. The coordinates of the non-hydrogen atoms are given in Table 2. See also ‘Supplementary material’.

Results

Synthesis of the catecholate complexes

Five-coordinate metal–catecholate complexes of the general formula [(triphos)M(Cat)]⁺ (M=Co(III), Rh(III) or Ir(III); Cat=Phen, Napht, DTBC, 4-MeCat,

TABLE 2. Atomic parameters for the structure of [(triphos)-Ir(OO)(PhenSQ)]BPh₄·0.5CH₂Cl₂^a

Atom	x	y	z	U or U _{eq}
Ir1	2278(0.6)	2243(0.4)	3324(0.4)	38(0.4)
P1	4171(3)	2670(2)	2789(2)	42(3)
P2	3326(4)	946(2)	3103(2)	48(3)
P3	1688(4)	2314(2)	2266(2)	48(4)
O1	1153(10)	3409(6)	3634(5)	56(3)
O2	2499(10)	2341(6)	4366(6)	60(3)
O3	624(10)	1928(6)	3868(6)	62(3)
O4A ^c	-189(27)	2548(17)	4287(15)	60(8)
O4B ^c	400(15)	2084(10)	4611(9)	58(4)
C1	5102(14)	2003(9)	2071(8)	106(5)
C2	3873(14)	819(8)	2159(8)	49(4)
C3	3097(14)	2166(9)	1525(8)	56(4)
C4	4277(14)	1566(9)	1714(8)	53(4)
C5	5172(15)	1267(9)	1017(8)	61(4)
C6	637(15)	3316(9)	4281(9)	58(4)
C7	1274(15)	2688(10)	4681(9)	59(4)
C8	1190(17)	2831(11)	5441(10)	72(5)
C9	118(19)	3404(12)	5759(11)	86(6)
C10	-734(18)	3920(11)	5339(10)	74(5)
C11	-396(16)	3928(10)	4628(9)	65(5)
C12	-1868(26)	4450(16)	5671(15)	120(9)
C13	-2524(29)	4959(17)	5218(17)	133(9)
C14	-2197(24)	5029(15)	4535(14)	106(8)
C15	-1124(19)	4479(12)	4211(11)	80(6)
C16	2090(22)	2414(13)	5794(12)	93(6)
C17	1969(30)	2569(18)	6490(17)	138(10)
C18	881(34)	3050(20)	6833(18)	157(11)
C19	-90(29)	3482(17)	6496(16)	131(9)
C2,1	6488(10)	2269(6)	3299(5)	61(4)
C3,1	7240(10)	2351(6)	3772(5)	78(5)
C4,1	6758(10)	2899(6)	4306(5)	91(6)
C5,1	5523(10)	3365(6)	4367(5)	108(7)
C6,1	4771(10)	3284(6)	3893(5)	84(6)
C1,1	5253(10)	2736(6)	3359(5)	47(4)
C2,2	5190(8)	3910(6)	1961(6)	68(5)
C3,2	5157(8)	4694(6)	1651(6)	80(6)
C4,2	3999(8)	5251(6)	1755(6)	77(5)
C5,2	2874(8)	5025(6)	2168(6)	82(6)
C6,2	2907(8)	4241(6)	2478(6)	57(4)
C1,2	4065(8)	3684(6)	2374(6)	49(4)
C2,3	2305(11)	-453(7)	3027(5)	77(5)
C3,3	1693(11)	-1097(7)	3336(5)	107(7)
C4,3	1215(11)	-1142(7)	4060(5)	101(7)
C5,3	1348(11)	-542(7)	4476(5)	88(6)
C6,3	1960(11)	102(7)	4167(5)	70(5)
C1,3	2438(11)	147(7)	3443(5)	56(4)
C2,4	4848(9)	921(5)	4106(5)	64(5)
C3,4	5883(9)	598(5)	4421(5)	71(5)
C4,4	6807(9)	-53(5)	4128(5)	84(6)
C5,4	6695(9)	-381(5)	3519(5)	83(6)
C6,4	5660(9)	-58(5)	3204(5)	69(5)
C1,4	4737(9)	593(5)	3498(5)	53(4)
C2,5	115(10)	1130(6)	2685(4)	62(4)
C3,5	-818(10)	702(6)	2593(4)	75(5)
C4,5	-1217(10)	784(6)	1958(4)	79(6)
C5,5	-683(10)	1294(6)	1414(4)	83(6)
C6,5	250(10)	1722(6)	1506(4)	76(5)
C1,5	649(10)	1640(6)	2141(4)	50(4)
C2,6	-537(10)	3430(6)	2561(5)	67(5)

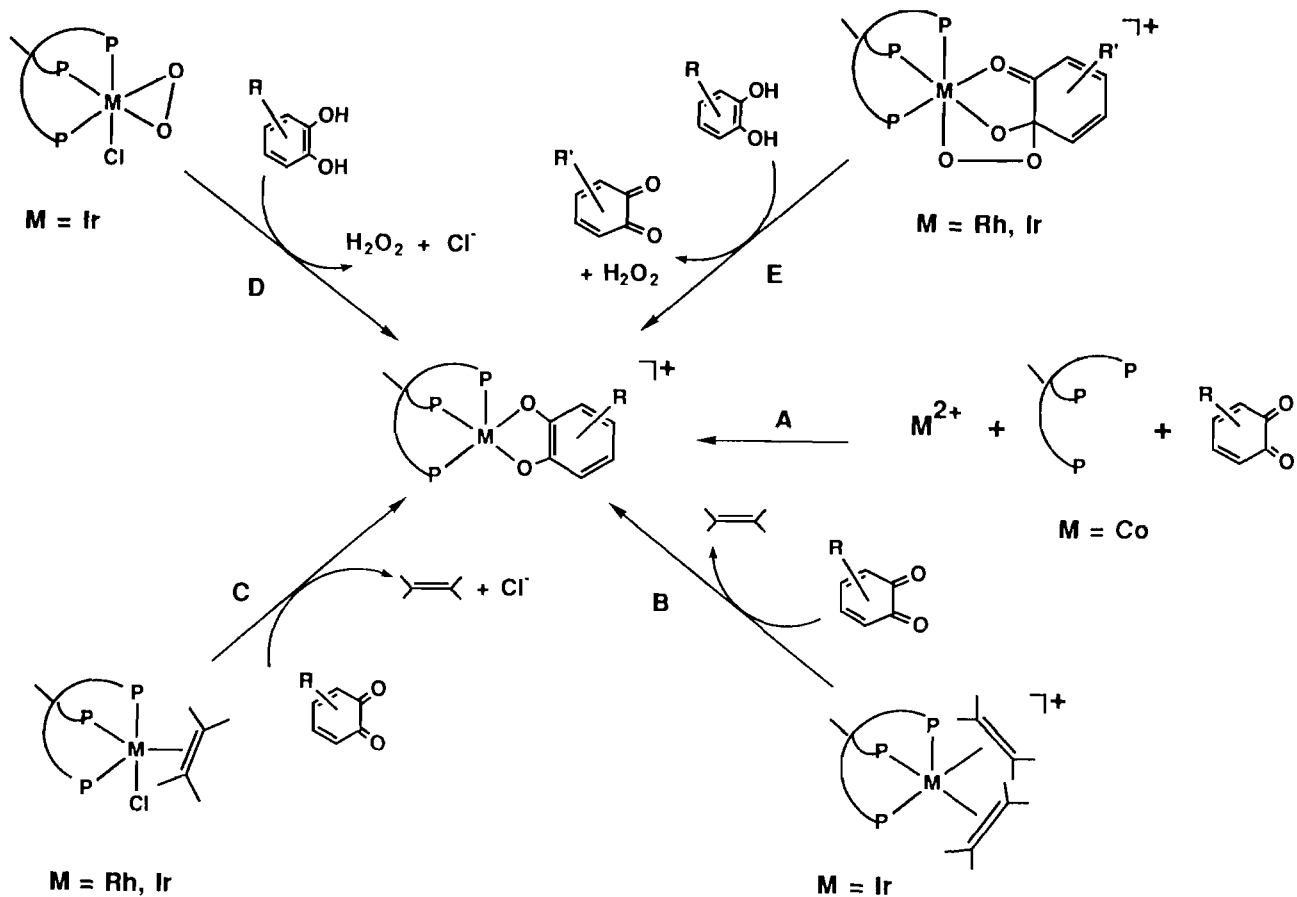
(continued)

TABLE 2. (continued)

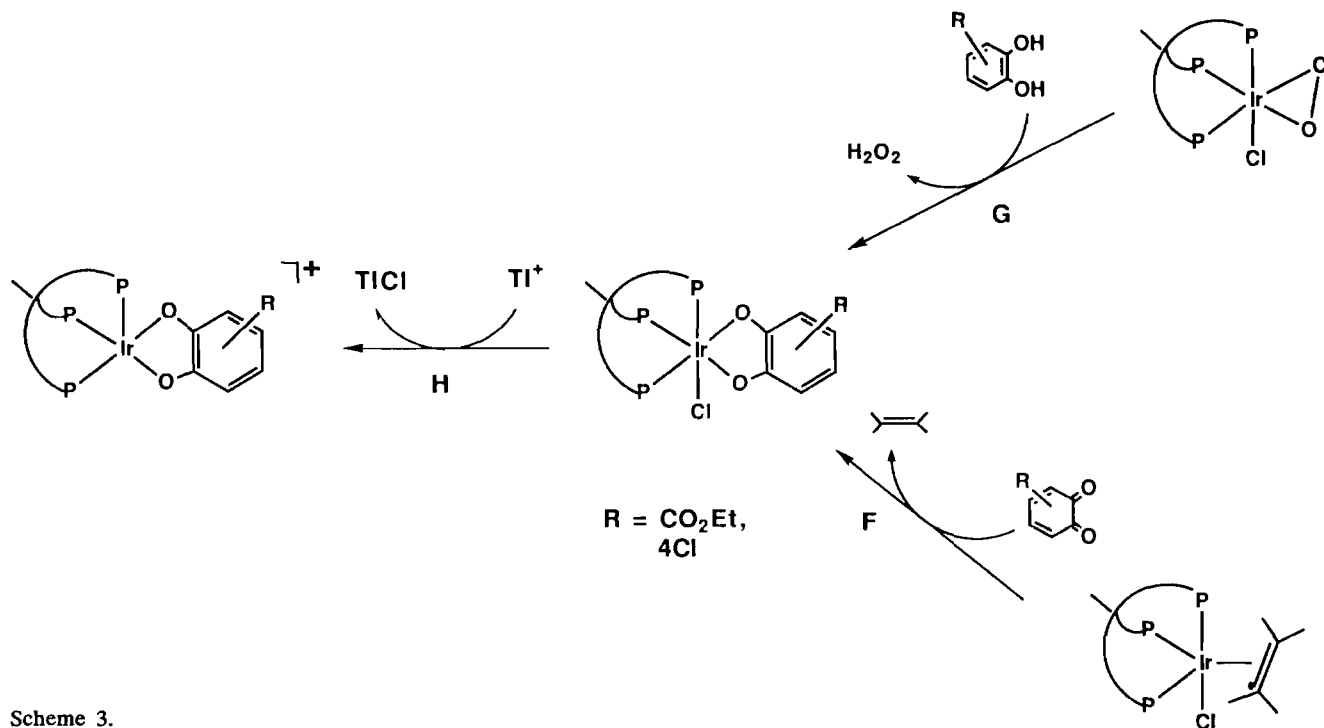
Atom	x	y	z	U or U _{eq}
C3,6	-1420(10)	4121(6)	2435(5)	92(6)
C4,6	-1091(10)	4647(6)	1856(5)	97(7)
C5,6	119(10)	4481(6)	1403(5)	99(7)
C6,6	1002(10)	3789(6)	1529(5)	69(5)
C1,6	673(10)	3264(6)	2108(5)	53(4)
B1	4263(19)	2327(12)	8625(10)	61(5)
C2,7	5642(9)	951(7)	9054(6)	69(5)
C3,7	6798(9)	446(7)	9124(6)	82(6)
C4,7	7975(9)	700(7)	8843(6)	98(7)
C5,7	7996(9)	1460(7)	8492(6)	97(7)
C6,7	6840(9)	1966(7)	8423(6)	79(5)
C1,7	5663(9)	1711(7)	8704(6)	64(5)
C2,8	5085(13)	2211(6)	7260(8)	105(7)
C3,8	5348(13)	2524(6)	6569(8)	120(8)
C4,8	5019(13)	3357(6)	6422(8)	139(9)
C5,8	4427(13)	3878(6)	6966(8)	121(8)
C6,8	4164(13)	3565(6)	7658(8)	82(6)
C1,8	4493(13)	2732(6)	7805(8)	62(5)
C2,9	2778(9)	3597(7)	9275(6)	71(5)
C3,9	2469(9)	4243(7)	9722(6)	86(6)
C4,9	3354(9)	4370(7)	10103(6)	81(5)
C5,9	4548(9)	3852(7)	10037(6)	81(5)
C6,9	4856(9)	3206(7)	9590(6)	65(5)
C1,9	3972(9)	3078(7)	9209(6)	51(4)
C210	2543(11)	1614(7)	8289(4)	73(5)
C310	1582(11)	1136(7)	8464(4)	97(6)
C410	1145(11)	890(7)	9163(4)	83(6)
C510	1669(11)	1122(7)	9687(4)	79(5)
C610	2631(11)	1601(7)	9512(4)	65(5)
C110	3067(11)	1847(7)	8813(4)	56(4)
C20	9092(34)	2769(22)	9564(20)	72(10)
C1A ^d	9302(24)	3465(15)	8767(13)	170(9)
C1A ^d	8810(28)	3472(18)	8998(16)	195(13)
C1B ^d	8094(21)	3100(12)	10421(11)	175(7)
C1B ^d	8935(24)	3345(14)	10198(13)	209(9)

^aThermal parameters multiplied by 1000, coordinates by 10000. ^bU_{eq} defined as one third of the trace of the orthogonalized thermal tensor. ^cThe refined population parameters of atoms O4A and O4B are 0.64(1) and 0.36(1), respectively, with their sum constrained to 1.0. ^dThe population parameters for the dichloromethane molecule is fixed to 0.5. The labels A and B refer to split images of the same atom.

EDHB or TClCat) can be obtained through different procedures, which are illustrated in Schemes 2 and 3. Cobalt complexes were prepared by a known one-pot reaction which involves mixing of equivalent amounts of Co²⁺ ions, triphos and *o*-quinones in CH₂Cl₂/*n*-butanol (path A) [2]. Rhodium and iridium complexes were obtained by either oxidative addition of *o*-quinones to Rh(I) [1] and Ir(I) complexes (paths B and C) or reaction of catechols with dioxygen adducts of the formula [(triphos)M(OO)(SQ)]⁺ (*vide infra*) (path E). The oxidative addition reactions of types B and C were carried out in CH₂Cl₂ solutions using Ir(I) and Rh(I) complexes with labile ligands such as [(tri-



Scheme 2.



Scheme 3.

phos)Ir(C₂H₄)₂]⁺ [6] or [(triphos)MCl(C₂H₄)] (M = Rh, Ir) [6, 7]. In the latter case, a chloride scavenger must be employed. Iridium complexes were prepared also by reaction of the peroxo complex [(triphos)IrCl(O₂)] [8] with catechols (path D).

Interestingly, six-coordinate chloro-catecholate complexes of the general formula [(triphos)IrCl(Cat)] are obtained from the reactions of [(triphos)IrCl(O₂)] and [(triphos)IrCl(C₂H₄)] with catechols and *o*-quinones, respectively (Scheme 3), bearing electron-withdrawing substituents (i.e. EDHBH₂ and TClQ; paths G and F). From the six-coordinate complexes, the corresponding five-coordinate species can be obtained by elimination of the chloride ligand with TlPF₆ (path H).

Characterization of the catecholate complexes

All of the five-coordinate complexes of the formula [(triphos)M(Cat)]⁺ (M = Co, Rh, Ir) exhibit quite similar spectroscopic (IR, NMR, UV) and electrochemical properties, and, therefore, are assigned the same primary structure in solution. In particular, the compounds are square pyramidal in the solid state as shown by an X-ray analysis carried out on the cobalt derivative [(triphos)Co(DTBC)]BPh₄ [2]. All of the five-coordinate complexes are soluble in common organic solvents in which they behave as 1:1 electrolytes (typical molar conductance values in 10⁻³ M nitroethane solution are 56 and 37 Ω⁻¹ cm² mol⁻¹ for BPh₄ and PF₆ derivatives, respectively). The six-coordinate complexes [(triphos)IrCl(Cat)] are soluble in acetone in which they behave as non-electrolytes.

The IR spectra of all compounds show no absorption in the region 1600–1700 cm⁻¹, where ν(C=O) stretching frequencies of coordinated *o*-quinones are generally observed (Table 3) [14, 15]. This indicates that the quinoid ligands are in their fully reduced catecholate form. Medium intensity bands at *c.* 1500 cm⁻¹ are assigned to the catecholate ring ν(C=C), while intense bands at *c.* 1300 cm⁻¹ are attributed to ν(C–O) of the coordinated catechols [16–27].

ESR and magnetic moment measurements in both the solid state and solution show all of these complexes to be diamagnetic.

³¹P{¹H} NMR data are reported in Table 4. All the spectra of the five-coordinate complexes are temperature-invariant in deaerated solutions in the range 308–173 K and consist of a singlet indicating an A₃ spin system, except for the Rh derivatives which show doublets (A₃X spin system) due to coupling of the three magnetically equivalent phosphorus nuclei to ¹⁰³Rh. Such patterns are consistent with a rapid intramolecular exchange of the three phosphorus atoms of triphos around the metal atom. A fluxionality of this type is commonly observed for five-coordinate triphos complexes and has been attributed to a fast intercon-

TABLE 3. Selected IR spectral data for Co, Rh and Ir catecholates and their dioxygen adducts^a

Complex	ν(C=C)	ν(C–O)	Substituent bands	Complex	ν(C=O)	ν(C=C)	ν(C–O)
[(triphos)Co(DTBC)] ⁺ ^b	^c	1230s, 1210s					
[(triphos)Co(Napht)] ⁺	1565m, 1548m	1210s					
[(triphos)Co(Phen)] ⁺	1590s	1245s					
[(triphos)Rh(EDHB)] ⁺	1574s	1280vs					
[(triphos)Rh(4-MeCat)] ⁺	1580s, 1510m	1303vs, 1282vs	1670vs ν(C=O)	[(triphos)Rh(O ₂)(NaphtSQ)] ⁺	1602m	1574s	1157s
[(triphos)Rh(DTBC)] ⁺	^c	1308s		[(triphos)Rh(O ₂)(PhenSQ)] ⁺	1610m	1591s, 1572vs	
[(triphos)Rh(Napht)] ⁺	1559s, 1507m	1308vs					
[(triphos)Rh(Phen)] ⁺	1559s, 1505m						
[(triphos)IrCl(TClCat)]	1524m	1261s	807s + 793 ν(C–Cl)				
[(triphos)Ir(TClCat)] ⁺	1515m	1268s					
[(triphos)IrCl(EDHB)]	1567s, 1556s	1290vs	1690vs + 1671vs ν(C=O)				
[(triphos)Ir(EDHB)] ⁺	1581s	1285vs	1694vs ν(C=O)				
[(triphos)Ir(4-MeCat)] ⁺	1571s, 1508m	1282s, 1260s		[(triphos)Ir(O ₂)(4-MeSQ)] ⁺	1641s	1562sh, 1556vs	1177s
[(triphos)Ir(DTBC)] ⁺ ^d	^c	1304s		[(triphos)Ir(O ₂)(DTBSO)] ⁺ ^d	1624s	1557sh, 1537vs	1194s, 1130vs
[(triphos)Ir(Napht)] ⁺	1556s, 1504m	1286vs, 1255vs		[(triphos)Ir(O ₂)(NaphtSQ)] ⁺	1601m	1572sh, 1556s	
[(triphos)Ir(Phen)] ⁺ ^d	1596s, 1510m			[(triphos)Ir(O ₂)(PhenSQ)] ⁺ ^d	1608m	1589s, 1564vs	1154s

^aNujol mulls; cm⁻¹. ^bData from ref. 2. ^cMasked by ν(C=C) triphos. ^dData from ref. 4.

TABLE 4. $^{31}\text{P}\{^1\text{H}\}$ NMR spectral data for catecholate complexes^a

Complex	Pattern	Chemical shift (ppm) ^b		Coupling constant, $J(\text{Hz})$	
		$\delta(\text{P}_A)$	$\delta(\text{P}_M)$	P_AP_M	P_AX
$[(\text{triphos})\text{Co}(\text{DTBC})]^+{}^c$	A_3	31.88			
$[(\text{triphos})\text{Co}(\text{Napht})]^+{}^c$	A_3	35.6(b)			
$[(\text{triphos})\text{Co}(\text{Phen})]^+{}^c$	A_3	36.9(b)			
$[(\text{triphos})\text{Rh}(\text{EDHB})]^+$	A_3X	34.70			107.2
$[(\text{triphos})\text{Rh}(4\text{-MeCat})]^+$	A_3X	32.62			109.5
$[(\text{triphos})\text{Rh}(\text{DTBC})]^+$	A_3X	32.29			110.7
$[(\text{triphos})\text{Rh}(\text{Napht})]^+$	A_3X	33.35			111.9
$[(\text{triphos})\text{Rh}(\text{Phen})]^+$	A_3X	33.39			115.0
$[(\text{triphos})\text{IrCl}(\text{TClCat})]^d$	AM_2	-25.68	-33.34	20.25	
$[(\text{triphos})\text{Ir}(\text{TClCat})]^d$	A_3	-24.12			
$[(\text{triphos})\text{IrCl}(\text{EDHB})]^+$	AM_2	-27.83	-35.65	20.50	
$[(\text{triphos})\text{Ir}(\text{EDHB})]^+$	A_3	-7.22			
$[(\text{triphos})\text{Ir}(4\text{-MeCat})]^+$	A_3	-7.77			
$[(\text{triphos})\text{Ir}(\text{DTBC})]^+{}^f$	A_3	-7.72			
$[(\text{triphos})\text{Ir}(\text{Napht})]^+$	A_3	-8.29			
$[(\text{triphos})\text{Ir}(\text{Phen})]^+{}^f$	A_3	-8.44			

^aAll spectra were recorded at room temperature (20 °C) in CDCl_3 deaerated solutions unless otherwise stated. ^bThe chemical shifts are relative to 85% H_3PO_4 at 0.00 ppm with positive values being downfield from the standard. ^cIn CD_2Cl_2 at 20 °C. ^dIn CD_3COCD_3 at 20 °C. ^eData from ref. 2. ^fData from ref. 4.

version between square pyramidal and trigonal bipyramidal geometries [7, 28–30]. The six-coordinate iridium compounds are rigid on the NMR time scale so that their $^{31}\text{P}\{^1\text{H}\}$ NMR spectra exhibit the expected AM_2 spin systems (Table 4).

The ^1H NMR spectra (CDCl_3 , 293 K) of the five-coordinate complexes are in line with the observed fluxionality. In fact, the three CH_2 groups of the skeleton of triphos appear magnetically equivalent (unique resonance centered in the range 2.5–2.8 ppm), while the resonance of the methyl substituent of triphos appears as a quartet in the range 1.3–1.8 ppm ($J(\text{HP}) \approx 3$ Hz). Selected ^1H NMR resonances due to the various catecholate substituents are reported in ‘Experimental’.

All of the electronic absorption spectra (CHCl_3 , 295 K) show an intense band in the range 240–320 nm and one or more less intense bands in the 350–850 nm region (Table 5). As an example, the spectrum of $[(\text{triphos})\text{Ir}(\text{DTBC})]\text{PF}_6$ is reported in Fig. 1(a). These features are similar to those observed for other metal catecholate complexes and are assigned to catecholate ligand $\pi \rightarrow \pi^*$ transitions and to LMCT (Cat \rightarrow M(III)) bands, respectively [15–18, 26, 31–43]. Indeed, the MO diagram for the present M(III) catecholate complexes is not qualitatively dissimilar from that already reported for $[(\text{PH}_3)_3\text{Co}(\text{Cat})]^+$ (Cat = $\text{H}_4\text{C}_6\text{O}_2$) [2]. Accordingly, the electronic transitions toward the LUMO (which is mainly metal $d_{\pi-1}$ in character with some contribution from the oxygen $p_{\pi-1}$ orbitals of the catecholate) can arise from either the deeper filled orbitals having a

strong metal t_{2g} character (therefore, these could be regarded as metal d–d transitions) or from higher energy orbitals having a strong contribution from the π orbitals of the catecholate ligand. In particular, we assign the lower energy band to the HOMO (π_{-1}) \rightarrow LUMO ($M-d_{\pi}$) transition (catecholate \rightarrow metal). This band is shifted to lower wavelength on going down the cobalt triad (as an example, the band is observed at 806, 724 and 571 nm for $[(\text{triphos})\text{M}(\text{DTBC})]^+$ derivatives of Co, Rh and Ir, respectively), while it decreases in energy on increasing the overall basicity of the catecholate ligands (for Ir complexes, the band is observed at 517, 517, 559, 571, 620 and 656 nm for TClCat, EDHB, 4Me-Cat, DTBC, Napht and Phen, respectively).

Electrochemistry of the catecholate complexes

In previous papers we have shown that cobalt and rhodium catecholate complexes of the formula $[(\text{triphos})\text{M}(\text{Cat})]^+$ (M = Rh, Cat = DTBC; M = Co, Cat = DTBC, Phen, TClCat) undergo electron-transfer reactions that encompass the M(III), M(II) and M(I) oxidation states of the metal, and the catecholate, semiquinonate and quinone oxidation levels of the quinoid ligand [1, 2]. This behavior is shared by all of the new $[(\text{triphos})\text{M}(\text{Cat})]^+$ complexes described in this paper (M = Co, Rh, Ir). Table 6 summarizes the main redox potential values. In following pages, we will discuss briefly the electrochemical behavior of the novel iridium derivatives, exemplified by $[(\text{triphos})\text{Ir}(\text{DTBC})]\text{PF}_6$, and

TABLE 5. UV-Vis spectral data at 22 °C for Co, Rh and Ir catecholates and their dioxygen adducts

Complex ^a	λ_{max} (nm) (ϵ_M (cm ⁻¹ mol ⁻¹ l))	Complex ^b	λ_{max} (nm) (ϵ_M (cm ⁻¹ mol ⁻¹ l))
[(triphos)Co(DTBC)] ⁺	258(18240); 374(sh); 430(sh); 614(sh); 806(3480)		
[(triphos)Co(Naphht)] ⁺	252(19260); 318(sh); 355(sh); 390(sh); 808(2550)		
[(triphos)Co(Phen)] ⁺	254(18900); 328(sh); 417(sh); 830(1070)		
[(triphos)Rh(EDHB)] ⁺	251(11240); 404(984); 636(1240)		
[(triphos)Rh(4-MeCat)] ⁺	255(22230); 420(1970); 694(3200)		
[(triphos)Rh(DTBC)] ⁺	247(20770); 293(sh); 424(1010); 724(3620)		
[(triphos)Rh(Naphht)] ⁺	258(28890); 430(sh); 794(5140)	[(triphos)Rh(O ₂)(NaphhtSO)] ⁺	265(18650); 354(sh); 512(sh)
[(triphos)Rh(Phen)] ⁺	254(26450); 309(sh); 394(sh); 813(3530)	[(triphos)Rh(O ₂)(PhenSO)] ⁺	255(22960); 310(sh); 387(sh)
[(triphos)Ir(TClCat)] ⁺	256(10060); 301(sh); 517(2020)		
[(triphos)Ir(EDHB)] ⁺	250(14860); 305(sh); 517(2650)		
[(triphos)Ir(4-MeCat)] ⁺	244(35160); 312(4360); 396(1820); 559(3490)		
[(triphos)Ir(DTBC)] ⁺	246(21310); 279(sh); 389(sh); 571(2970)	[(triphos)Ir(O ₂)(DTBSO)] ⁺	248(22210); 270(sh); 278(sh); 378(sh)
[(triphos)Ir(Naphht)] ⁺	256(18870); 317(4690); 410(sh); 620(750)	[(triphos)Ir(O ₂)(NaphhtSO)] ⁺	255(22930); 318(sh); 367(sh); 418(sh)
[(triphos)Ir(Phen)] ⁺	252(37590); 278(sh); 308(sh); 387(sh); 656(3070)	[(triphos)Ir(O ₂)(PhenSO)] ⁺	246(40410); 300(10010); 371(2270)

^aIn CHCl₃, deaerated solutions c. 10⁻⁴ M. ^bIn CHCl₃, oxygenated solutions c. 10⁻⁴ M. ^cData from ref. 4.

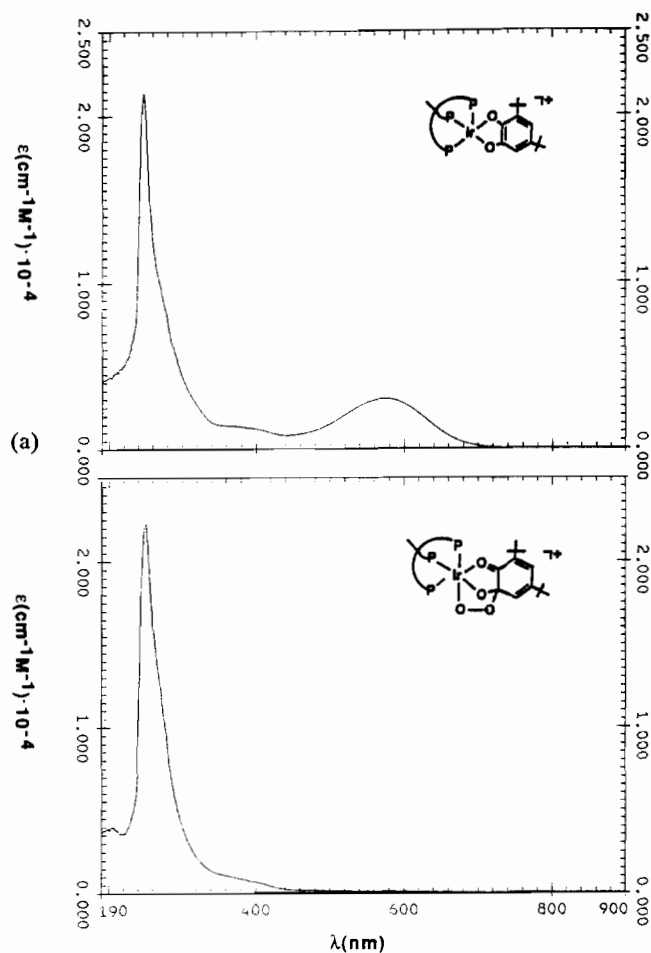


Fig. 1. UV-Vis spectra (CHCl₃, 295 K) of [(triphos)Ir(DTBC)]PF₆ in deaerated solution (a) and in oxygenated solution (b).

will report the X-band ESR characterization of some paramagnetic species, namely the semiquinone complexes [(triphos)Ir(DTBSO)]²⁺ and [(triphos)Ir(PhenSO)]²⁺ and the Ir(II) complex [(triphos)Ir(DTBC)] that can be generated by controlled potential macroelectrolysis. The latter complexes are of particular importance since Ir(II) compounds are very rare species and very little ESR characterization is available [44].

Figure 2(a) illustrates the electron-transfer ability exhibited by [(triphos)Ir(DTBC)]PF₆ in deaerated acetonitrile solution. The complex undergoes two subsequent oxidations as well as two subsequent reduction processes. Both the two anodic steps and the first cathodic step display a directly associated response in the reverse scan. In contrast, the second reduction process shows features of chemical irreversibility. Controlled potential coulometric tests proved each charge transfer to involve one electron/molecule. As anticipated, this redox pathway is in agreement with the trend already observed for metal d⁶ catecholate com-

TABLE 6. Formal electrode potentials (V) for the redox changes exhibited by Co, Rh and Ir catecholate complexes $[(\text{triphos})\text{M}(\text{Cat})]^+$ in MeCN solution at $-20\text{ }^\circ\text{C}^{\text{a}}$

Complex	$\text{M}^{\text{III}}(\text{Q})/\text{M}^{\text{III}}(\text{SQ})$	$\text{M}^{\text{III}}(\text{SQ})/\text{M}^{\text{III}}(\text{Cat})$	$\text{M}^{\text{III}}(\text{Cat})/\text{M}^{\text{II}}(\text{Cat})$	$\text{M}^{\text{II}}(\text{Cat})/\text{M}^{\text{I}}(\text{Cat})$
$[(\text{triphos})\text{Co}(\text{DTBC})]^{+\text{b,e}}$	+1.04 ^f	+0.73	-0.49	-1.63 ^f
$[(\text{triphos})\text{Co}(\text{Napht})]^+$	+0.90 ^f	+0.70 ^g	-0.47	ⁿ
$[(\text{triphos})\text{Co}(\text{Phen})]^+$	+0.77 ^g	+0.66 ^g	-0.53	ⁿ
$[(\text{triphos})\text{Rh}(\text{EDHB})]^{+\text{h}}$	+1.25 ^f	+0.79	-0.61	-1.45 ^g
$[(\text{triphos})\text{Rh}(4\text{-MeCat})]^+$	+1.05 ^f	+0.34	-0.67 ^f	-1.45 ^g
$[(\text{triphos})\text{Rh}(\text{DTBC})]^{+\text{c,m}}$	+0.94 ^f	+0.28	-0.78	-1.56 ^g
$[(\text{triphos})\text{Rh}(\text{Napht})]^+$	+0.88 ^f	+0.21	-1.24 ^f	ⁿ
$[(\text{triphos})\text{Rh}(\text{Phen})]^+$	+0.77 ^f	+0.13	-0.69	-1.50 ^g
$[(\text{triphos})\text{Ir}(\text{TCICat})]^{+\text{h}}$	^p	+0.93	-0.74 ^f	ⁿ
$[(\text{triphos})\text{Ir}(\text{EDHB})]^{+\text{c,h}}$	^p	+0.84	-0.85 ^f	ⁿ
$[(\text{triphos})\text{Ir}(4\text{-MeCat})]^{+\text{h}}$	+1.30 ^f	+0.70	-1.01 ^g	ⁿ
$[(\text{triphos})\text{Ir}(\text{DTBC})]^{+\text{d}}$	+1.10 ^f	+0.25	-1.05 ^h	-1.83 ^g
$[(\text{triphos})\text{Ir}(\text{Napht})]^+$	+0.83 ^f	+0.18 ^f	-1.24 ^g	ⁿ
$[(\text{triphos})\text{Ir}(\text{Phen})]^{+\text{d}}$	+0.87 ^f	+0.11	-0.96 ^g	ⁿ

^aKey: Q = *o*-quinonate; SQ = *o*-semiquinonate; Cat = catecholate. ^bData from ref. 2. ^cData from ref. 1. ^dData from ref. 4. ^eAt $20\text{ }^\circ\text{C}$. ^fInstable. ^gPeak potential value for irreversible processes. ^hIn CH_2Cl_2 . ^mAt $-15\text{ }^\circ\text{C}$. ⁿComplicated due to slow decomposition. ^pNot observed due to solvent oxidation.

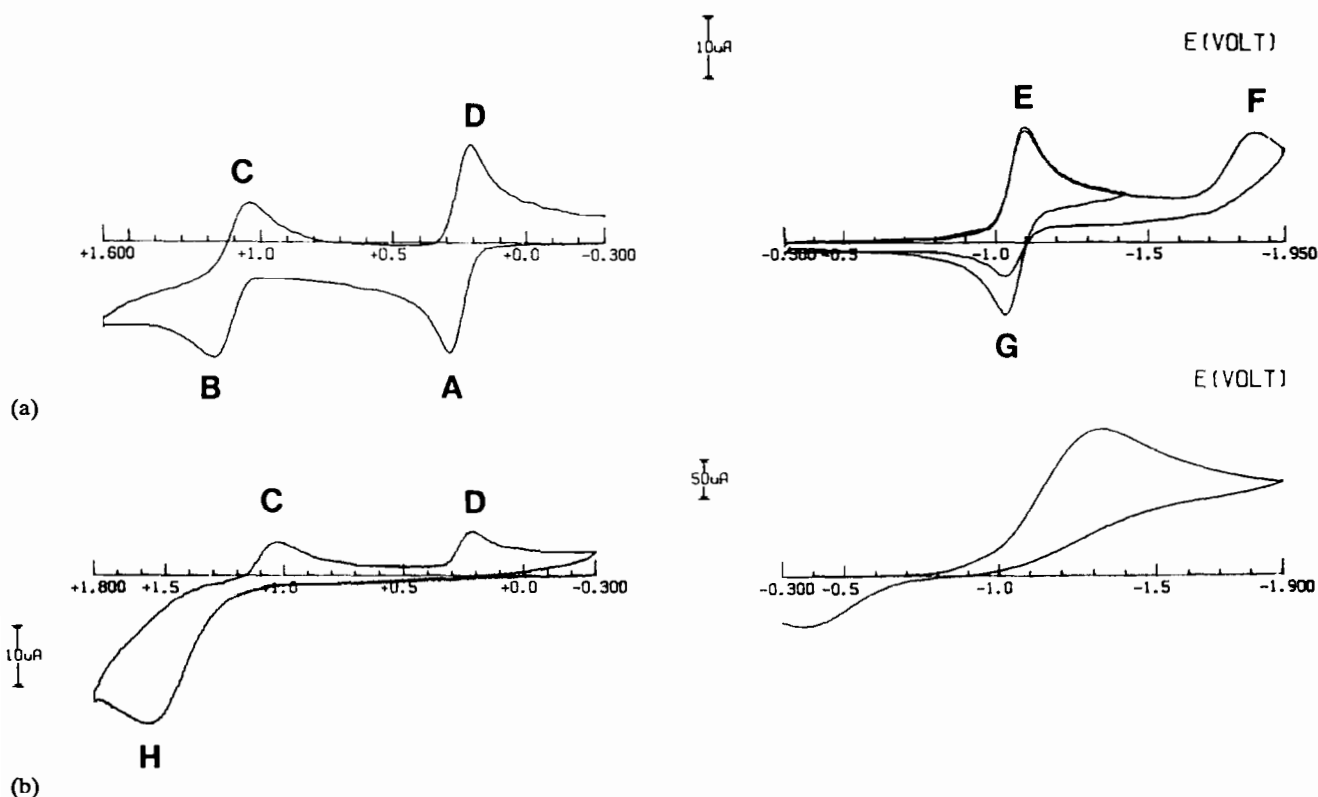
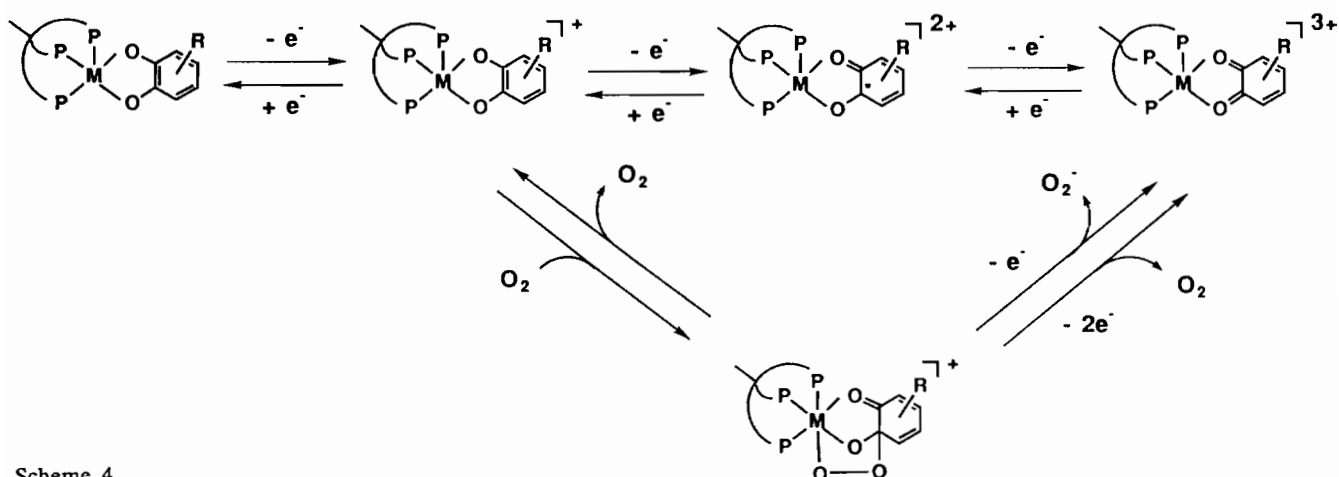


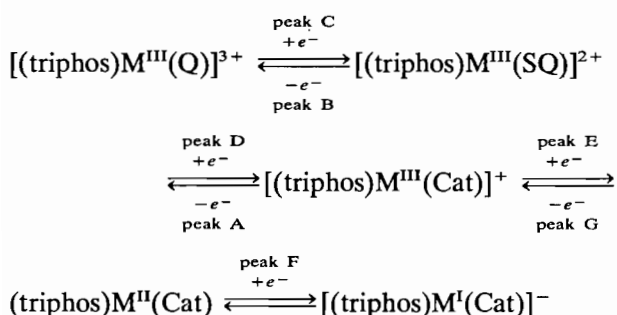
Fig. 2. Cyclic voltammetric responses recorded at a platinum electrode on a MeCN solution containing $[(\text{triphos})\text{Ir}(\text{DTBC})]\text{PF}_6$ ($1.31 \times 10^{-3}\text{ mol dm}^{-3}$) and Et_4NClO_4 (0.1 mol dm^{-3}). Scan rate 0.2 V s^{-1} . $T = -20\text{ }^\circ\text{C}$. (a) Deaerated solution; (b) solution after bubbling O_2 for 10 min.

plexes of triphos, which commonly exhibit the ligand-centered catecholate \rightleftharpoons semiquinone \rightleftharpoons quinone sequence (Scheme 4), together with two metal-centered

electron transfers [1, 2, 45, 46]. In conclusion, the overall redox pattern is attributable to the following redox changes:



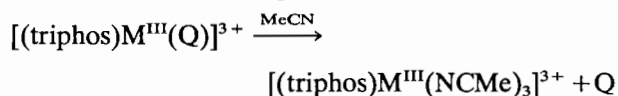
Scheme 4.



The general MO diagram previously reported [2] well justifies the above electrochemical pattern since both the π_{\perp} and π_{\perp}^* levels (HOMO and LUMO for $[(\text{triphos})M(\text{Cat})]^+$ complexes) are allowed to be empty, singly or doubly populated. This variable electron population induces a different extent of the metal–ligand π_{\perp} interaction but does not destroy the primary geometry of the complexes.

Analysis of the cyclic voltammetric responses relevant to the peak-system A/D with scan rates varying from 0.02 to 20.48 V s^{-1} , shows that: (i) the $i_{p(D)}/i_{p(A)}$ ratio is constantly equal to 1; (ii) the $i_{p(A)}v^{-1/2}$ term is substantially constant; (iii) the peak-to-peak separation ΔE_p progressively increases from 67 to 264 mV. If one consider that, under the same experimental conditions, the one-electron oxidation of ferrocene ($E^{\circ'} = +0.38$ V) exhibits a quite coincident trend of ΔE_p with scan rate, rather than the theoretically expected constant value of 59 mV (likely because of some uncompensated solution resistance), it can be assumed that the catechol–semiquinone oxidation involves a chemically and electrochemically reversible electron transfer; (iv) the cyclic voltammetric response recorded after exhaustive electrolysis at this first anodic step ($E_w = +0.50$ V) shows that the peak-system A/D is now reversed.

As far as the semiquinone–quinone oxidation is concerned (peak-system B/C), the current ratio $i_{p(C)}/i_{p(B)}$ is lower than unity (about 0.8 at 0.2 V s^{-1} , at 10 °C). This feature is shared by the peak-systems B/C of all the Co, Rh and Ir complexes examined here. A temperature increase further lowers this parameter; on the other hand the current ratios assume the value of 1 independently on the scan rate at -20 °C, indicating that the chemical complications responsible for the slow decomposition of the electrogenerable $[(\text{triphos})M^{\text{III}}(\text{Q})]^{3+}$ species are totally quenched. Exhaustive two-electrons oxidations at the appropriate potentials of $[(\text{triphos})M^{\text{III}}(\text{Cat})]^+$, give rise to cyclic voltammetric responses fully consistent with the following decomposition pathway [1, 2]:



Nevertheless, subsequent exhaustive reductions at 0.00 V completely restore the starting catechol species.

As for the ability of $[(\text{triphos})M^{\text{III}}(\text{Cat})]^+$ to uptake electrons, the diagnostic electrochemical parameters relative to the peak-system E/G testify a reversible, chemically and electrochemically, M(III)/M(II) redox change in almost all the cases (see Table 6), showing that the first reduction step does not destroy the starting framework. Finally, the irreversibility of the Ir(II)/Ir(I) redox change, peak F in Fig. 2(a), precluding to the destruction of the starting molecular frame, induced us to neglect any further investigation.

ESR characterization of Ir(III) semiquinone and Ir(II) catechol complexes

In view of the electrochemical results, both the Ir(III) semiquinone complex $[(\text{triphos})\text{Ir}(\text{DTBSQ})]^{2+}$ and the Ir(II) catechol $[(\text{triphos})\text{Ir}(\text{DTBC})]$ are expected to

be easily generated. Indeed, the exhaustive electrolysis of **1b** in MeCN at $-20\text{ }^{\circ}\text{C}$ at 0.50 V (0.2 mol dm^{-3} $[\text{NBu}_4]\text{ClO}_4$ as supporting electrolyte) gave a paramagnetic product which was examined by X-band ESR spectroscopy.

The frozen solution spectrum in MeCN (Fig. 3(a)) shows a well resolved axial structure with $g_{\perp} > g_{\parallel}$ ($g_{\perp} = 2.010$, $g_{\parallel} = 1.973$) and an overall linewidth $\Delta H_{100\text{K}}$ of 74 G . These features are consistent with the preferential localization of the unpaired electron on the quinoid ligand [2, 34, 42]. The absence of any hyperfine resolution in the lineshape is consistent with no appreciable interaction of the unpaired electron with either the Ir nucleus ($I = 3/2$) or the three phosphorus nuclei of triphos. The presence of a semiquinone ligand in the complex is confirmed by the room temperature spectrum reported in Fig. 3(b) (second-derivative). The following coupling constants have been introduced to reproduce the spectrum, which appears as a doublet of quartets: $\langle A_{\text{H}} \rangle = 3.8\text{ G}$ (H being the *meta* hydrogen of DTBC) and $\langle A_{\text{P}} \rangle \approx 1.8\text{ G}$ (P being the three phosphorus of triphos). The quartet splitting

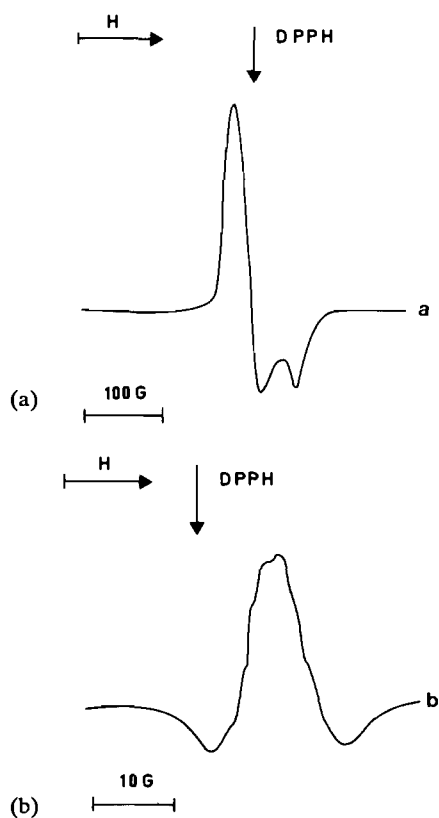


Fig. 3. X-band ESR spectra of a MeCN solution of $[(\text{triphos})\text{Ir}(\text{DTBC})]\text{PF}_6$ exhaustively electrolyzed at $E_w = 0.50\text{ V}$ at 253 K (0.2 mol dm^{-3} $[\text{Bu}_4\text{N}]\text{ClO}_4$ as supporting electrolyte): (a) first-derivative spectrum at 100 K ; (b) second-derivative spectrum at 300 K .

might be due also to coupling of the unpaired electron to the ^{193}Ir and ^{191}Ir nuclei. However, we exclude this interpretation in light of the ESR spectra of the rhodium analogue $[(\text{triphos})\text{Rh}(\text{DTBSQ})]^{2+}$ [1] and of the Ir(II) derivative $[(\text{triphos})\text{Ir}(\text{DTBC})]$ (see below). Both coupling constants and $\langle g \rangle$ values are clearly indicative of a radical species in which the unpaired electron is largely localized on the semiquinone ligand [47]. Quite similar spectral features are shown by the electrogenerated semiquinone complex $[(\text{triphos})\text{Ir}(\text{PhenSQ})]^{2+}$ (MeCN, $-20\text{ }^{\circ}\text{C}$, $E_w = 0.50\text{ V}$) confirming that the one-electron oxidation of the Ir(III) catecholates is centered at the quinoid ligands (ESR parameters in MeCN frozen solution: axial structure with $g_{\perp} = 2.007$, $g_{\parallel} = 1.984$, $\Delta H_{100\text{K}} = 48\text{ G}$, $\langle g_{\text{calc}} \rangle = 1.997$; fluid solution 300 K : $\langle g \rangle = 2.001$, $\langle \Delta H \rangle = 15\text{ G}$).

In contrast, the addition of one electron to the Ir(III) catecholate complexes results in the reduction of Ir(III) to Ir(II). The frozen solution spectrum of electrogenerated (MeCN, $-20\text{ }^{\circ}\text{C}$, $E_w = -1.3\text{ V}$) $[(\text{triphos})\text{Ir}(\text{DTBC})](\text{MeCN}, 100\text{ K})$ is reported in Fig. 4(a). The spectrum can be interpreted by using a $S = 1/2$ spin Hamiltonian with $g_{\perp} = 2.062$ ($A_{\perp} = 238\text{ G}$) and $g_{\parallel} = 1.960$ ($A_{\parallel} = 310\text{ G}$). A three-line resolution is pres-

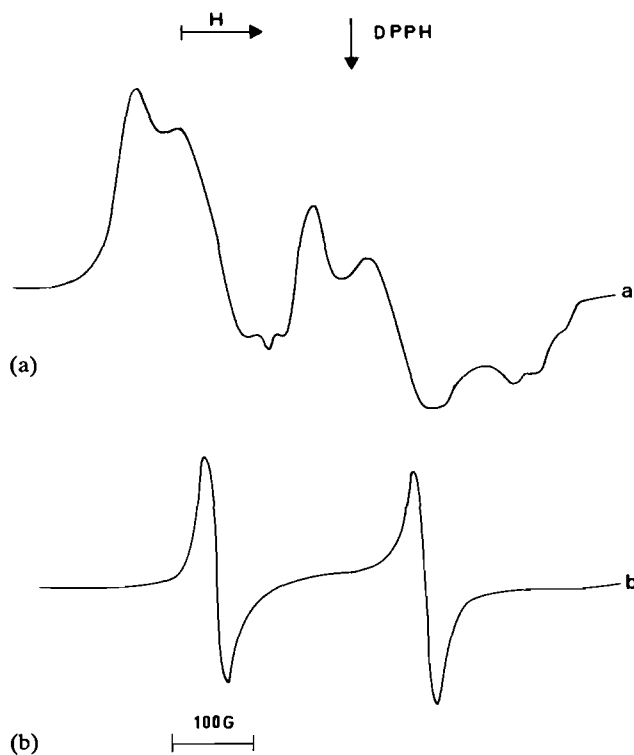


Fig. 4. X-band ESR spectra of a MeCN solution of $[(\text{triphos})\text{Ir}(\text{DTBC})]\text{PF}_6$ exhaustively electrolyzed at $E_w = -1.30\text{ V}$ at 253 K (0.2 mol dm^{-3} $[\text{Bu}_4\text{N}]\text{ClO}_4$ as supporting electrolyte): (a) first-derivative spectrum at 100 K ; (b) first-derivative spectrum at 300 K .

ent in each perpendicular ($A_{\perp}=60$ G) and parallel ($A_{\parallel}=31$ G) absorption. The spectrum is comparable with those of a number of low-spin square pyramidal Rh(II) complexes stabilized by tripodal polyphosphine ligands, including the strictly related [(triphos)Rh(DTBC)] complex [1]. Indeed, the set of ESR parameters shown by [(triphos)Ir(DTBC)] is diagnostic for a square pyramidal symmetry with the unpaired electron in the d_{z^2} orbital [48]. Accordingly, the large A_{\perp} and A_{\parallel} values are assigned to a strong interaction of the unpaired electron with the apical phosphorus, which faces the d_{z^2} SOMO [29, 49]. The three-line splitting in the perpendicular and parallel absorptions is attributed to appreciable interaction of the electron with the two basal phosphorus nuclei; in contrast no appreciable coupling to the metal is observed. The isotropic spectrum of the Ir(II) catechololate is shown in Fig. 4(b) (MeCN, 300 K). It consists of a doublet at $\langle g \rangle = 2.026$, indicating strong coupling between the unpaired electron and one phosphorus nucleus only ($\langle A_{\perp} \rangle = 260$ G). No superhyperfine structure is observed even by a second-order derivative analysis, probably due to fast molecular tumbling at room temperature.

Synthesis of the oxygenated complexes

All of the dioxygen adducts of the general formula [(triphos) $\overline{M}(\text{OO})(\text{SQ})$]Y (Y = BPh₄, PF₆) were prepared by bubbling O₂ through a CH₂Cl₂ solution of the corresponding catechololate derivative at the appropriate temperature (see below) (Scheme 4). The formation of the dioxygen adducts occurs also in the dark. In all cases, the occurrence of a reaction was put in evidence by a fast color change. Most of the dioxygen adducts can be isolated in the solid state by addition of *n*-butanol to the CH₂Cl₂ solutions. These complexes behave as 1:1 electrolytes in solution and are diamagnetic in both the solid state and solution (Evans' method, ESR evidence).

Characterization of the oxygenated complexes

Crystal structure

The crystal structure of [(triphos)Ir(OO)(PhenSQ)]BPh₄·0.5CH₂Cl₂ (**4a**) has been determined by X-ray methods. Selected bond angles and lengths are reported in Table 7. In the complex cation (Fig. 5), the metal is octahedrally coordinated by the three phosphorus atoms of triphos and by three oxygen atoms, two from the original catechololate ligand that has attained a semiquinoid structure, and one from O₂ which bridges the metal and a carbon atom of the quinoid ligand. Indeed, the addition of O₂ has clearly induced a rearrangement of the π -bonding structure inner to the quinoid ligand. Thus, a double bond is localized at the C6–O1 atoms (distance 1.26(2) Å), while the C6–C7

TABLE 7. Selected bond and distances (Å) and angles (°) for [(triphos)Ir(OO)(PhenSQ)]BPh₄·0.5CH₂Cl₂

Ir–P1	2.263(4)	P1–Ir–P2	86.2(1)
Ir–P2	2.307(4)	P1–Ir–P3	91.7(1)
Ir–P3	2.280(5)	P2–Ir–P3	85.3(1)
Ir–O1	2.19(1)	P1–Ir–O1	99.1(3)
Ir–O2	2.14(1)	P1–Ir–O2	94.0(3)
Ir–O3	1.97(1)	P1–Ir–O3	174.4(3)
O1–C6	1.26(2)	P2–Ir–O1	173.9(3)
O2–C7	1.37(2)	P3–Ir–O2	168(3)
O3–O4A	1.47(2)	O1–Ir–O2	72.2(4)
O3–O4B	1.43(3)	Ir–O1–C6	111(2)
O4A–O4B	1.13(3)	Ir–O2–C7	103.0(9)
C7–O4A	1.54(3)	Ir–O3–O4A	116.6(1)
C6–O4B	1.71(4)	Ir–O3–O4B	114(1)
C6–C7	1.40(2)	O3–O4A–C7	110(1)
		O3–O4B–C6	111(2)
		O1–C6–C7	114(1)
		O2–C7–C6	117(1)

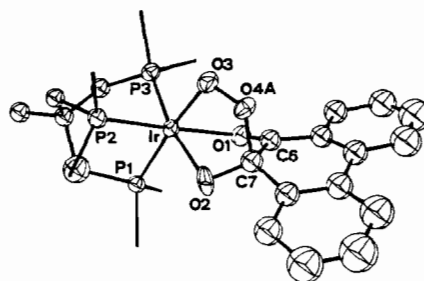


Fig. 5. ORTEP drawing of the complex cation [(triphos)Ir(OO)(PhenSQ)]⁺ in **4a**. The split image of atom O_{4A} (i.e. O_{4B}) is not shown and also the phenyl rings are omitted for clarity.

and C7–O2 linkages acquire more single bond character (1.40(2) and 1.37(2) Å, respectively). The metalocycle Ir–O3–O4A–C7–O2 is clearly featured in Fig. 5, although a disordered orientation of the oxygen molecule (based upon the refinement of site occupancy factors) allows a residual 35% probability of closing the metalocycle over the atom C6, which is chemically equivalent to C7. The preferential binding of the distal oxygen atom to C7 reflects an enhancement of the incipient sp³ hybridization at C7 (sum of the in-plane angles: 345° at C7 versus 358° at C6). Analogously, the C7 atom is more displaced than C6 out of the catechololate plane (0.32 versus 0.09 Å). The relatively small difference excludes, however, possible macroscopic effects on the temperature factors of the two carbon atoms that could be imposed by the disordered situation. Remarkably, the O4A–C7 (1.54(3) Å) linkage is shorter than O4B–C6 (1.71 Å) involving a more trigonal pyramidal carbon. The fact that even the shorter separation is at least 0.12 Å longer the average C–O single bond [50] indicates here a very atypical bond.

There are two stereocenters in each molecule (the iridium and the sp³ carbon atom of the semiquinolate

ligand) that, being interconnected, originate only two possible stereoisomers. The observed disorder suggests that an interconversion of each stereoisomer into its equivalent one is possible with the distal oxygen atom moving over the C6–C7 bond.

As a final remark, the quinoid ligand is not perfectly planar as the dihedral angle between the chelating part (O–C–C–O) and the system of three condensed C6 rings is *c.* 24°. Moreover, the least-squares plane of the overall ligand is tilted by *c.* 43° with respect to the equatorial plane of the pseudooctahedron at the metal. In this way the physical separation between the metal and the C(O) atom is reduced and the closure of the five-membered metallocycle by O₂ is facilitated.

Spectroscopy

By a comparison of the chemico-physical properties, one can readily conclude that all of the dioxygen adducts of the present metal catecholates share their primary structure with 4a in both the solid state and solution. In particular, the O₂-promoted ketonization of a C–O bond of the parent catecholate ligands is shown by the IR spectra (Table 3), which exhibit strong $\nu(\text{C}=\text{O})$ absorptions approximately 50 cm⁻¹ lower than those of the corresponding free quinones [14, 15]. Strong bands in the 1100–1200 cm⁻¹ region can be assigned to $\nu(\text{C}_{\text{sp}^3}-\text{O})$ [51]. The solution spectra (CHCl₃) remain practically unchanged with respect to those recorded in Nujol mulls, thus showing that the compounds retain the same structure in both the solid state and solution.

The ³¹P{¹H} NMR spectra (Table 8) show that the interaction of the metal catecholates with dioxygen removes the magnetic equivalence of the phosphorus atoms of triphos. Indeed, three different resonances

(AMQ or AMQX spin systems, X = Rh) are now observed, except for the PhenSQ derivatives which display AB₂ or AB₂X spin systems. All of the patterns are invariant in the temperature range in which each dioxygen adduct is stable. The AB₂ pattern of the PhenSQ complexes can be interpreted in terms of the existence of two stereoisomers as mentioned above, and, particularly, by a fast interconversion of each stereoisomer into its equivalent one by simple moving of the distal oxygen atom over the (O)C–C(O) bond. The apparent rigidity of all of the other complexes (temperature-invariant AMQ or AMQX patterns) suggests a preferential binding of O₂ at one of the two catecholate C–O carbon atoms. However, due to the asymmetry of all of the quinoid ligands but Phen, the inequivalence of the phosphorus atoms would be observable also for a fast equilibrium involving shuttling back and forth of the oxygen atom between the two (O)C–C(O) carbon atoms.

Details of the ¹H NMR spectra for all of the compounds are given in 'Experimental'.

Table 5 summarizes the UV–Vis spectral data. It is worth noticing that as a consequence of the dioxygen uptake, the bands in the 350–850 nm region disappear, a fact that is in agreement with their assignment to HOMO(π_{\perp}) → LUMO(π_{\perp}^*) transitions (Fig. 1(b)). Interestingly, the uptake of dioxygen by [(triphos)M(Cat)]⁺ complexes appears related to the frequency of the LMCT (HOMO → LUMO) absorptions occurring in the visible region. In particular it is observed that, on diminishing the energy gap between the ligand and metal orbitals, the formation of dioxygen adducts is thermodynamically easier. This finding is rich in interesting implications as LMCT bands in metal ca-

TABLE 8. ³¹P{¹H} NMR spectral data for catecholate–dioxygen adducts^a

Complex	Pattern	Chemical shift (ppm) ^b			Coupling constant, J(Hz)					
		$\delta(\text{P}_A)$	$\delta(\text{P}_M)$	$\delta(\text{P}_O)$	P_AP_M	P_AP_O	P_MP_O	P_AX	P_MX	P_OX
[(triphos)Co(O ₂)NaphtSQ] ⁺	AM ₂	33.2(b)	27.7(b)		r					
[(triphos)Co(O ₂)(PhenSQ)] ⁺	AM ₂	34.5(b)	25.4(b)		r					
[(triphos)Rh(O ₂)(4-MeSQ)] ⁺ ^d	AMQX	22.37	14.33	11.99	37.1	44.3	33.5	124.4	98.7	99.6
[(triphos)Rh(O ₂)(DTBSQ)] ⁺ ^e	AMQX	19.53	11.93	7.77	46.3	35.9	35.3	117.7	105.5	98.9
[(triphos)Rh(O ₂)(NaphtSQ)] ⁺ ^e	AMQX	21.19	14.67	12.27	35.5	48.1	32.8	121.8	99.2	105.6
[(triphos)Rh(O ₂)(PhenSQ)] ⁺ ^c	A ₂ MX	18.30	12.90		34.7			112.2	99.5	
[(triphos)Ir(O ₂)EDHBSQ] ⁺ ^m	AMQ	-25.00	-26.32	-27.72	19.2	21.0	25.8			
[(triphos)Ir(O ₂)(4-MeSQ)] ⁺ ^d	AMQ	-24.95	-27.21	-28.48	19.0	20.7	25.8			
[(triphos)Ir(O ₂)(DTBSQ)] ⁺ ^h	AMQ	-25.11	-26.80	-28.84	20.6	26.6	19.3			
[(triphos)Ir(O ₂)(NaphtSQ)] ⁺	ABC	-25.29	-27.91 ^f	-28.63 ^g	19.8 ⁿ	19.5 ^p	26.4 ^q			
[(triphos)Ir(O ₂)(PhenSQ)] ⁺ ^h	AB ₂	-25.65	-26.90 ^f		19.2 ⁿ					

^aAll spectra were recorded at room temperature (20 °C) in CDCl₃ oxygenated solutions unless otherwise stated. ^bThe chemical shifts are relative to 85% H₃PO₄ with positive values being downfield from the standard. ^c-20 °C. ^d-50°C. ^e-30 °C. ^f $\delta(\text{P}_B)$. ^g $\delta(\text{P}_C)$. ^hData from ref. 4. ^mIn CD₂Cl₂ at -70 °C. ⁿJ(P_AP_B). ^pJ(P_AP_C). ^qJ(P_BP_C). ^rNot measured due to quadrupolar effects.

techolates have been related to the Lewis acidity of the metal center [52] and to its ability to react with dioxygen [53].

Electrochemistry of the oxygenated complexes

When dioxygen is bubbled into a deaerated MeCN solution of a $[(\text{triphos})\text{M}(\text{Cat})]^+$ complex at -20°C , three types of voltammetric responses are observed:

(i) The voltammetric responses remain unchanged with respect to those of the catechol derivatives, showing that the compounds do not react with O_2 in these experimental conditions. Such behavior is displayed by $[(\text{triphos})\text{Ir}(\text{Cat})]^+$ (Cat = EDHB, TClCat); $[(\text{triphos})\text{Rh}(\text{EDHB})]^+$; $[(\text{triphos})\text{Co}(\text{Cat})]^+$ (Cat = Napht, DTBC).

(ii) The voltammetric responses show the disappearance of the $\text{M}^{\text{III}}(\text{Cat})/\text{M}^{\text{III}}(\text{SQ})$ process, while the $\text{M}^{\text{III}}(\text{SQ})/\text{M}^{\text{III}}(\text{Q})$ step is still present. In this case, it is sufficient to bubble N_2 again into the solution to restore the voltammetric responses characteristic of the starting catechol complexes. The fact that in the reverse scan the $\text{M}^{\text{III}}(\text{SQ})/\text{M}^{\text{III}}(\text{Cat})$ reduction peak is again observable even under O_2 (Fig. 6 illustrates this behavior for $[(\text{triphos})\text{Rh}(4\text{-MeCat})]^+$) is consistent with the release of the superoxide ion from a transient $[(\text{triphos})\text{M}(\text{OO})(\text{SQ})]^{2+}$ species that spontaneously and rapidly converts to $[(\text{triphos})\text{M}(\text{Q})]^{3+}$ and O_2^- (the formation of O_2^- is proved by the X-band ESR spectra which display the typical signal at $\langle g \rangle = 2.007$) [54]. This behavior is observed by $[(\text{triphos})\text{Ir}(4\text{-MeCat})]^+$ and $[(\text{triphos})\text{Rh}(\text{Cat})]^+$ (Cat = DTBC, 4-MeCat) (Scheme 4).

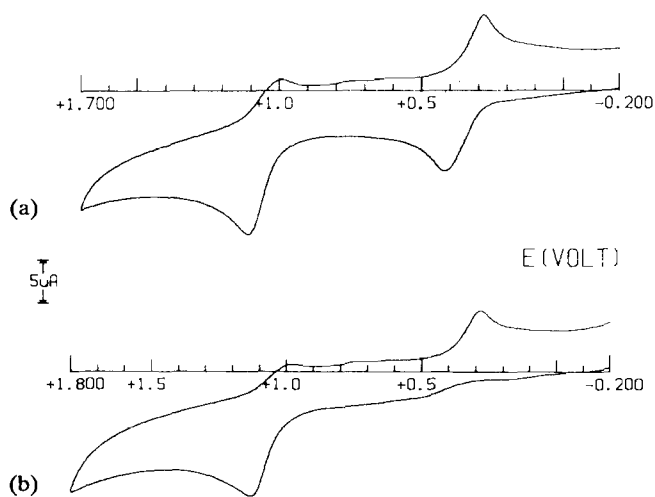


Fig. 6. Cyclic voltammograms recorded at a platinum electrode on a MeCN solution containing $[(\text{triphos})\text{Rh}(4\text{-MeCat})]\text{PF}_6$ ($1.9 \times 10^{-3} \text{ mol dm}^{-3}$) and Et_4NClO_4 (0.1 mol dm^{-3}). Scan rate 0.2 V s^{-1} . $T = -20^\circ\text{C}$. (a) Deaerated solution; (b) solution after bubbling O_2 for 10 min.

(iii) The remaining catechol complexes exhibit a third behavior. As exemplified in Fig. 2(b) for $[(\text{triphos})\text{Ir}(\text{DTBC})]^+$, bubbling dioxygen into a MeCN solution causes evident variations in the voltammetric profiles with respect to those shown in Fig. 2(a). Both $\text{Ir}^{\text{III}}(\text{Cat})/\text{Ir}^{\text{III}}(\text{SQ})$ and $\text{Ir}^{\text{III}}(\text{SQ})/\text{Ir}^{\text{III}}(\text{Q})$ oxidation processes disappear while a new irreversible oxidation peak is observed at much more positive potential values (peak H in Fig. 2(b)). However, the reduction $\text{Ir}^{\text{III}}(\text{Q}) \rightarrow \text{Ir}^{\text{III}}(\text{SQ}) \rightarrow \text{Ir}^{\text{III}}(\text{Cat})$ processes (peaks C and D in Fig. 2(b)) exhibited by the deoxygenated compound are clearly regenerated in the reverse scan. As for the cathodic region, the reduction of the excess of dioxygen obscures any cathodic process of the oxygenated product. Full elucidation of the overall electrode mechanism is provided by an analysis of the electrochemical behavior of the dioxygen adduct of $[(\text{triphos})\text{Ir}(\text{Phen})]^+$ which is stable under a dinitrogen atmosphere.

As shown in Fig. 7, this adduct undergoes, in deaerated MeCN solution, both an irreversible oxidation at peak H ($E_p = +1.55 \text{ V}$) and an irreversible reduction at peak I ($E_p = -0.96 \text{ V}$). As in the case of $[(\text{triphos})\text{Ir}(\text{OO})(\text{DTBSQ})]^+$, the anodic process generates a species which is reversibly reduced in correspondence to peaks C and D, respectively. In light of this evidence, one can hypothesize this species to be $[(\text{triphos})\text{Ir}(\text{PhenQ})]^{3+}$, the peak systems C/B and D/A being attributable to the redox changes $[(\text{triphos})\text{Ir}(\text{PhenQ})]^{3+}/[(\text{triphos})\text{Ir}(\text{PhenSQ})]^{2+}$ ($E^{\circ'} = +0.87 \text{ V}$) and $[(\text{triphos})\text{Ir}(\text{PhenSQ})]^{2+}/[(\text{triphos})\text{Ir}(\text{Phen})]^+$ ($E^{\circ'} = +0.11 \text{ V}$), respectively. As a matter of fact, controlled potential coulometry ($E_w = +1.7 \text{ V}$, versus Ag/AgCl) consumes two electrons/molecule

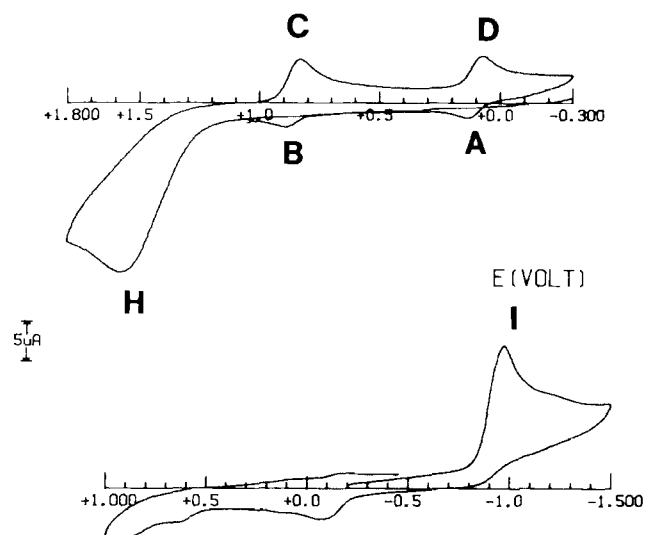


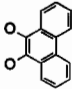
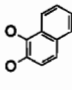
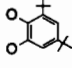
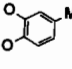
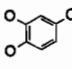
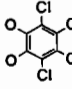
Fig. 7. Cyclic voltammograms recorded at a platinum electrode on a deaerated MeCN solution containing $[(\text{triphos})\text{Ir}(\text{OO})(\text{PhenSQ})]\text{PF}_6$ ($1.57 \times 10^{-3} \text{ mol dm}^{-3}$) and Et_4NClO_4 (0.2 mol dm^{-3}). Scan rate 0.2 V s^{-1} . $T = -20^\circ\text{C}$.

and affords a solution which exhibits a cyclic voltammogram readily attributable to $[(\text{triphos})\text{Ir}(\text{PhenQ})]^{3+}$ (Scheme 4). In contrast to the chemical reversibility of the anodic removal of oxygen, the reduction process of the oxygenated product (peak I in Fig. 7), which involves one electron/molecule, does not lead to the starting deoxygenated congener. In fact, the exhaustively reduced solution, which is ESR silent, gives rise to a voltammetric picture attributable only to fragmentation products.

Table 9 summarizes the voltammetric behavior of the catecholate complexes in oxygenated solutions together with the peak potentials at which the two-electron or one-electron removals are observed.

Inspection of the data reported in Table 9 reveals that the potentials of the couples $M^{\text{III}}(\text{SQ})/M^{\text{III}}(\text{Cat})$ appear related to the kind of voltammetric behavior exhibited by the oxygenated complexes, with the exception of $[(\text{triphos})\text{Co}(\text{OO})(\text{PhenSQ})]\text{ClO}_4$. In fact, complexes which have potential values larger than +0.70 V do not react with dioxygen at -20°C , those which have potential values between +0.70 and +0.28 V show a behavior of type (ii), and those which have potential values lower than +0.28 V exhibit a behavior of type (iii).

TABLE 9. Voltammetric behavior of $[(\text{triphos})\text{M}(\text{Cat})]^+$ complexes in oxygenated MeCN solutions at -20°C (The potentials of the couples $M^{\text{III}}(\text{Cat})/M^{\text{III}}(\text{SQ})$ in deaerated solutions are reported in parentheses^b)

Cat	Ir	Rh	Co
	III +1.55 (+0.11)	III +1.50 (+0.13)	III +1.35 (0.66)
	III +1.20 (+0.18)	III +1.40 (+0.21)	I (+0.70)
	III +1.55 (+0.25)	II +0.94 (0.28)	I (+0.73)
	II +1.30 (0.70)	II +1.06 (0.34)	
	I (-0.84)	I (+0.79)	
	I (+0.93)		

^aKey: I = behavior of type (i) (see text), II = behavior of type (ii), III = behavior of type (iii). Values reported are the peak potentials relative to either bielectronic or mono-electronic oxidations (in volts). ^bValues in parentheses are taken from Table 6.

Factors affecting the dioxygen uptake by metal catecholates

As will be apparent in forthcoming pages, a number of factors can affect the dioxygen uptake by metal catecholates of the general formula $[(\text{triphos})\text{M}(\text{Cat})]^+$ to give the dioxygen adducts $[(\text{triphos})\text{M}(\text{OO})(\text{SQ})]^+$. These factors are deeply interwoven with one another and, therefore, should be considered altogether. However, an analysis of this type might likely generate some confusion, particularly on the role played by each factor, hence we will consider them separately.

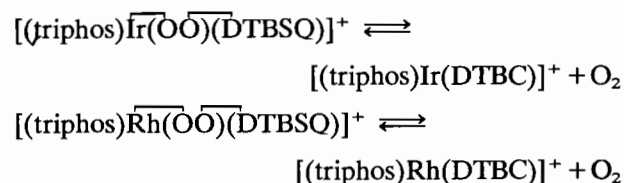
Nature of the metal and of the catecholate ligand

At a fixed temperature (see next paragraph), the ease with which a metal catecholate complex picks up dioxygen increases on going from catecholate ligands bearing electron-withdrawing substituents to catecholate ligands bearing electron-releasing substituents. In other words, the more basic the catecholate ligand (Phen > Naph > DTBC > 4MeCat > EDHB > TClCat), the easier is the dioxygen uptake (when the dioxygen uptake occurs, it is invariably an immediate reaction). Interestingly, for each catecholate ligand, the dioxygen uptake is favored on going from cobalt to iridium (see 'Discussion').

Temperature and pressure

The various dioxygen adducts have different stabilities in solution depending on the temperature. Thermal stabilities in oxygen-saturated solutions were determined by correlating the composition of the reaction mixture (³¹P NMR sealed tubes) versus the variation of the temperature in the range 173–373 K. Each oxygenated complex shows a well defined range of existence: beyond that point, a further increase in the temperature promotes the release of dioxygen and converts each adduct to the corresponding catecholate complex. The temperature ranges in which each complex exists in O₂-saturated solutions as oxygenated form only, catecholate form only or both of them, are illustrated in Fig. 8. Due to the nature of either the metal or catechol, the complexes $[(\text{triphos})\text{Co}(\text{DTBC})]^+$, $[(\text{triphos})\text{Rh}(\text{EDHB})]^+$ and $[(\text{triphos})\text{Ir}(\text{TClCat})]^+$ do not form a dioxygen adduct even at the lowest temperature attained (173 K).

The equilibrium constants K for the interconversions:



have been calculated at different temperatures by ³¹P NMR integration in the temperature ranges 30 to 60

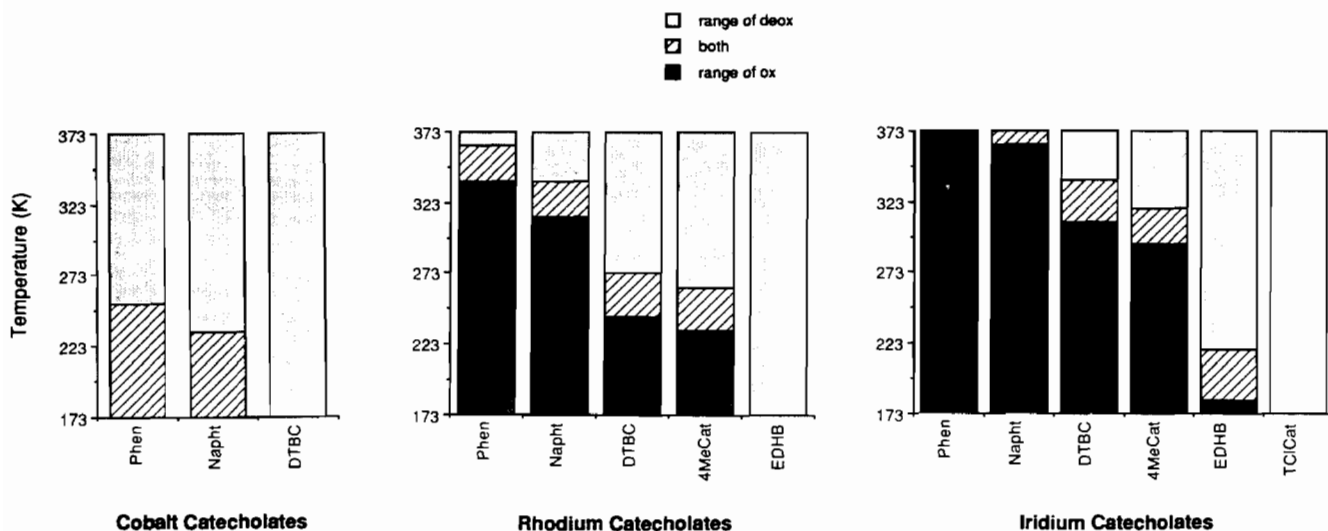


Fig. 8. Temperature range of existence of Co, Rh and Ir dioxygen adducts and their dioxygen-free complexes in oxygen saturated solutions.

°C and -10 to -35 °C for Ir and Rh, respectively (oxygen-saturated sealed tubes). The log K values have been plotted against $1/T$ giving a satisfactory linear least-squares regression in both cases (with a correlation coefficient of 99.8% and 99.9%, respectively). The interpolating functions allow one to calculate the enthalpy and entropy values for the reactions. The thermodynamic functions (Table 10) for the two conversions are rather similar with each other indicating a reaction mechanism of the same type. It is also evident that the Rh complex (not isolated in the solid state) which was erroneously assigned an 'open' structure [1], actually shares the same primary geometry with the iridium analog. From a perusal of the thermodynamic data shown in Table 10, one may readily observe the following: (i) the oxygen release is endothermic, which is consistent with the temperature effect; (ii) the ΔS° values are largely positive and consistent with a dissociative reaction.

At room temperature, the catecholates complexes can be classified into three categories: complexes which form a dioxygen adduct and do not lose O_2 even under anaerobic conditions, complexes which form a dioxygen adduct but lose O_2 by bubbling N_2 into their solutions,

TABLE 10. Thermodynamic functions for the conversion of 3,5-di-tert-butylcatecholate dioxygen adducts complexes into their dioxygen-free derivatives

Metal	ΔH_R^a	ΔS_R^a	ΔG_R (298 K)
Ir	21.2 ± 0.2	62.5 ± 0.8	2.58 ± 0.04
Rh	19.7 ± 0.5	74 ± 2	-2.4 ± 0.1

^aAssumed temperature independent in the range examined.

and complexes which never pick up O_2 . To the first class belong the Rh and Ir catecholates with Napht and Phen, while to the second class belong the Ir catecholates with DTBC and 4MeCat which, therefore, add and lose reversibly dioxygen by bubbling O_2 and N_2 , respectively. Finally, the complexes of the third class react with dioxygen at high dioxygen pressures only. The effect of the pressure is shown in Fig. 9 for the reaction of $[(\text{triphos})\text{Rh}(\text{DTBC})]^+$ with O_2 at 5 atm. The dotted line represents the IR spectrum of $[(\text{triphos})\text{Rh}(\text{DTBC})]^+$ in a deaerated dichloroethane solution at 25 °C, while the continuous line corresponds

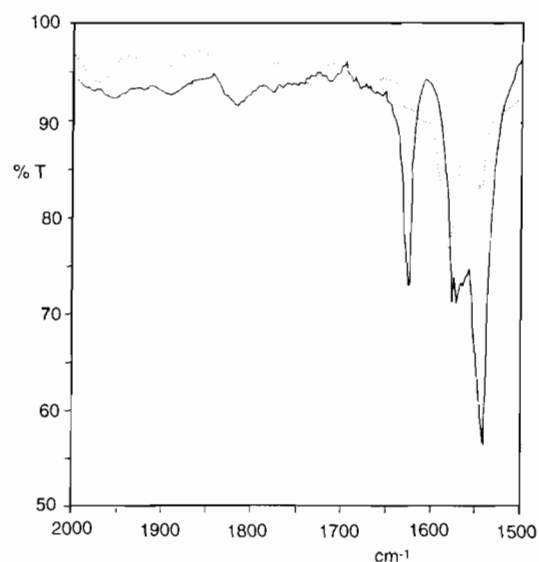


Fig. 9. IR solution spectra of $[(\text{triphos})\text{Rh}(\text{DTBC})]^+$ (dotted line; deaerated solution, 25 °C) and $[(\text{triphos})\text{Rh}(\text{OO})(\text{DTBSQ})]^+$ (solid line; 1 atm O_2 , -10 °C or 5 atm O_2 , 25 °C).

to the spectrum recorded at 5 atm of O₂. At the latter pressure, [(triphos)Rh(OO)(DTBSQ)]⁺ forms as shown by the strong band at 1620 cm⁻¹ (ν(C=O)), and by the absorption enhancement at 1540 cm⁻¹. The same spectrum is observed under 1 atm of O₂ at -10 °C.

Free coordination site at the metal

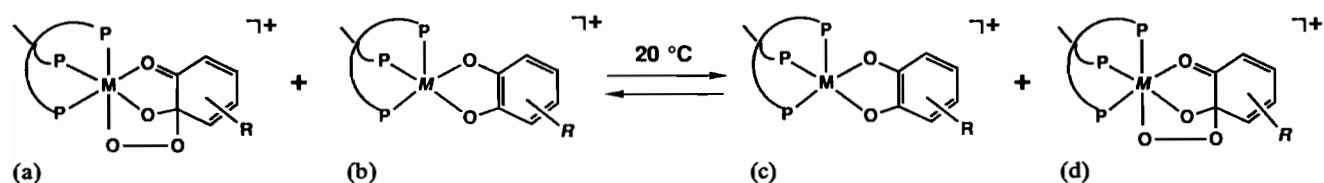
All of the five-coordinate catecholates complexes are 16-electron species only formally since the metal π₁ (A) fragment orbital accepts part of the electron density located in the catecholate's 3b₁ FMO [2]. In other words, the catecholate ligand can be the donor of a third electron pair (of π₁ type). Nevertheless, the complexes can be considered coordinatively unsaturated species with a free coordination site at the metal. The importance of this vacancy is clearly shown by the fact that the six-coordinate complex [(triphos)IrCl(EDHB)] does not form a dioxygen adduct even at a very low temperature (173 K) or at high pressure of O₂ (50 atm). In contrast, the dioxygen adduct [(triphos)Ir(OO)(EDHBSQ)]⁺ can be obtained at 188 K after removing the chloride ligand from [(triphos)IrCl(EDHB)] with a chloride scavenger (Scheme 3). Notice that the formation of the six-coordinate complexes occurs only with catecholate ligands bearing electron-withdrawing substituents and, therefore, not sufficiently basic to stabilize the five-coordinate species via π-interaction.

Solvent

The dioxygen uptake by [(triphos)M(Cat)]⁺ complexes does not appear to be affected by the nature of the solvent. A large variety of solvents have been tested such as CH₂Cl₂, CHCl₃, CH₃NO₂, acetone, DMF and MeCN.

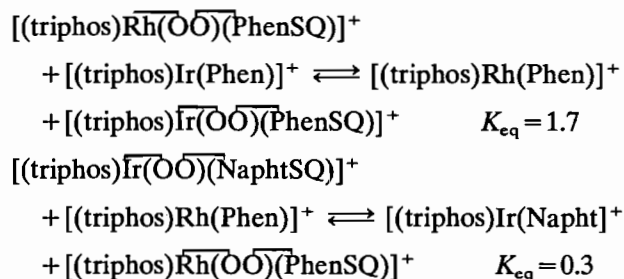
Oxygen transfer between metal catecholates

Even in the conditions of thermodynamic stability, a dioxygen adduct [(triphos)M(OO)(SQ)]⁺ (a) can release dioxygen in solution when it is allowed to react under nitrogen with a catecholate complex, [(triphos)M'(Cat')]⁺ (b) which has a greater affinity for dioxygen (Scheme 5). As a result, [(triphos)M(Cat)]⁺ (c) and [(triphos)M'(OO)(SQ')]⁺ (d) are formed. ³¹P NMR analysis of the reaction mixture shows the solution to contain all the species involved in the dioxygen exchange. In other words, a chemical equilibrium holds



Scheme 5.

in which dioxygen is preferentially bonded to the complex which forms a more stable dioxygen adduct. As an example, the reactions (deaerated solutions, 20 °C) involving Ir and Rh complexes with Napht and Phen gave the following equilibrium constants:



$$K_{\text{eq}} = [c][d]/[a][b]$$

The observed effect of temperature and O₂ pressure on the dioxygen uptake is clearly consistent with an equilibrium involving the dioxygen adducts and their catecholate form (Scheme 4). Such an equilibrium well accounts for the oxygen-transfer reactions, i.e. the reaction with a catecholate complex having a higher affinity for dioxygen shifts the equilibrium of Scheme 5 to the right.

Discussion

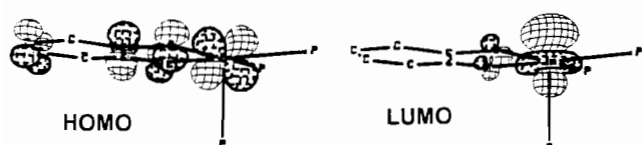
The formation of dioxygen metal complexes is a topic of much current interest because of the many unsolved questions regarding the mechanism. In the following discussion we will try to adapt some of the already proposed mechanisms to our system and, finally, we shall propose a new reaction pathway that stems from experimental facts and theoretical MO ideas. The latter, derived from specific EHMO calculations [55], are descriptively presented here but the computational details will be reported elsewhere [56].

A widely accepted model for the attack of a dioxygen molecule to a metal center is the spin pairing model [57]. According to the latter, a triplet O₂ molecule pairs one spin with that of a paramagnetic metal center either in the ground state (e.g. Co²⁺ d⁷) or via excited states (if the number of d electrons is even). At this point and for the sake of subsequent arguments, it is worth noticing that there is no experimental evidence whatsoever that the five-coordinated catecholate com-

plexes under investigation have easy access to paramagnetic ground states. This is consistent with the large HOMO-LUMO gaps in the range 1.1–1.6 eV calculated for the models of $[(\text{triphos})\text{M}(\text{Cat})]^+$ complexes ($\text{M} = \text{Co}, \text{Rh}, \text{Ir}$). A large HOMO-LUMO separation can also be estimated from electrochemical data, namely from the E° values relative to the one-electron oxidation to $[(\text{triphos})\text{M}(\text{SQ})]^{2+}$ and to the one-electron reduction to $[(\text{triphos})\text{M}(\text{Cat})]$ (Table 6). By supposing, however, that an electron can still be promoted from the HOMO to the LUMO, the system would acquire the features of a diradical $\text{M}(\text{II})\text{-SQ}$. In fact the two levels in question have catecholate (π) and metal character, respectively, as clearly shown by the three-dimensional CACAO drawings [58] in Scheme 6.

If a paramagnetic species is attained, no matter how energetically expensive, the mechanism suggested by Cox and Que for the dioxygen uptake by iron(III) catecholates (Scheme 7) could be adapted to our system as well. In fact, the latter involves an inner-sphere charge transfer that gives a diradical $\text{Fe}(\text{II})\text{-SQ}$ species, which is appropriate to interact with paramagnetic O_2 . Interestingly, intermediate A (not seen) has a structure quite similar to that of our dioxygen adducts [53].

Once again it is worth mentioning the lack of any experimentally observed paramagnetism for our $[(\text{triphos})\text{Co}(\text{cat})]^+$ species² (ESR, Evans' method), while

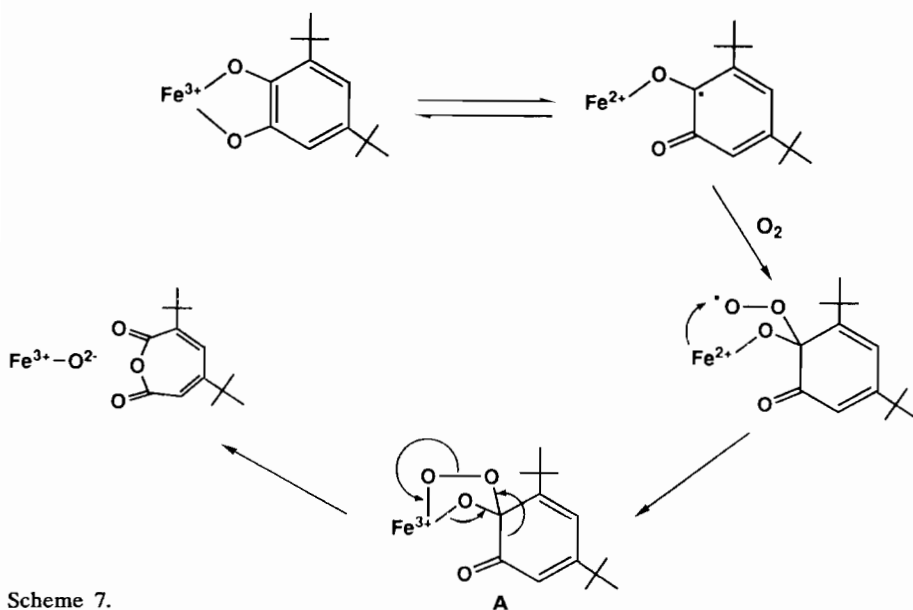


Scheme 6.

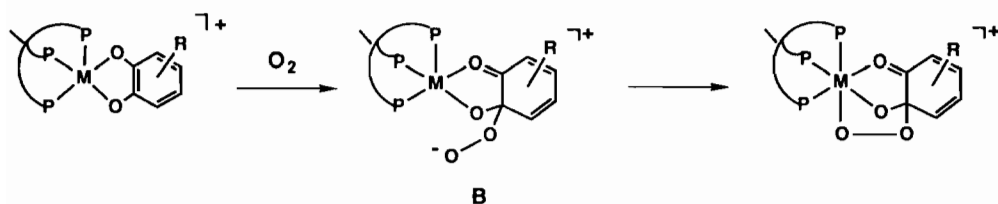
their d^6 $\text{M}(\text{III})$ catechololate character is evidenced by the NMR chemical shifts, the X-ray structure of $[(\text{triphos})\text{Co}(\text{DTBC})]^+$, and the E° values associated with the complexed Cat/SQ couples. The latter are considerably more positive than those reported for the free ligands (this large positive shift indicates that the coordination of the catechols to the d^6 metal centers significantly stabilizes the catecholate oxidation state) [2].

In conclusion, to be consistent with the proposal of Que, who also had no direct evidence for $\text{Fe}(\text{II})\text{-SQ}$ species, one should hypothesize for our complexes a small contribution of the $\text{M}(\text{II})\text{-SQ}$ form, so small to leave the structural and NMR parameters virtually unperturbed.

If the spin pairing models are difficult to accept for the reasons given, alternative mechanisms can be proposed, more or less convincingly supported by the crop of experimental data presented above. One of these, is based on the fact that the precursor five-coordinate complexes $[(\text{triphos})\text{M}(\text{cat})]^+$ have a free coordination site at the metal in the absence of which no reaction with O_2 occurs. Accordingly, one could conclude that O_2 attacks initially the square pyramidal metal center (16 electrons) and, in a second step, it closes the metallocycle by making a new bond with one catecholite $\text{C}(\text{O})$ carbon atom. This mechanism has a major weak point based on the low capability of dioxygen to behave as a nucleophile, it being best recognized as an electrophile. Thus another, more reasonable, mechanism is the one involving initial attack of O_2 at one $\text{C}(\text{O})$ carbon atom, followed by the closure of the $\text{M}-\text{O}-\text{C}-\text{O}-\text{O}$ metallocycle (Scheme 8). In this case the electrophilicity of the O_2 molecule should be exerted



Scheme 7.



Scheme 8.

toward the catecholate ligand and, in particular, toward the C(O) atoms or their π -bonding interregion. Indeed, the HOMO (Scheme 6) has a slight predominance at the latter atoms but, in actuality, it is delocalized over the whole ligand. Under these circumstances, it is somewhat difficult to emphasize (at least in MO terms) the regioselectivity of the attack.

The delocalization of the catecholate π_{\perp} system seems to have a critical role in the reactivity toward O_2 . Thus, the nature of the catecholate itself is a governing factor, the best effects being obtained with condensed rings and/or electron-donor substituents that can affect the contribution of the O and C(O) atoms to the HOMO and, in turn, the accumulation of electron density at them. Within this context, the optimum effect is achieved with 9,10-phenanthrenecatecholate where the presence of two external aromatic rings disfavors resonance structures with a single bond between the two C(O) atoms. In contrast complexes with catecholate ligands bearing electron-withdrawing substituents (i.e. TICat or EDHB) either form the least stable O_2 adducts or do not react with O_2 at all.

Also, the nature of the metal itself can be related to the amount of electron density accumulated at the catecholate and its C(O) atoms. Recall, in fact, that in the five-coordinate $L_3M(\text{cat})^+$ complexes [2] there is a π_{\perp} donor-acceptor relation between the HOMO of catecholate and a suitably hybridized d_{\perp} metal FMO. The antibonding counterpart of the latter interaction is barely visible in the LUMO of Scheme 6, even though rehybridization effects confer to the metal $\sigma(z^2)$ more than a d_{π} character. The lower is the energy of the metal orbital ($\text{Co} < \text{Rh} < \text{Ir}$), the smaller is the gap with the catecholate HOMO, the better is the metal-ligand π interaction. As a consequence, the Co(III) ion is privileged in receiving the donation of two electrons (of π_{\perp} type) from the catecholate and formally better attains the 18-electron count. By contrast, a weaker interaction leaves Ir(III) much more acidic and, in turn, the catecholate ligand more basic or electron richer.

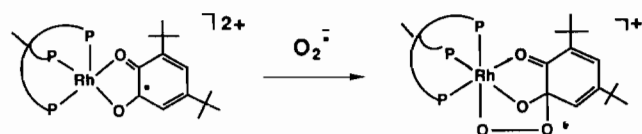
The above arguments are all consistent with the experimental facts that the heavier are the metals and the more electron rich is the catecholate (at the OCCO region), the better is the reaction with O_2 . If the reaction proceeds by steps, the first impact of O_2 with the electron rich catecholate molecule can initially favour

the formation of adduct B in Scheme 8. Subsequently, the free end of O_2 can interact with the metal. Indirect support to the latter mechanism could be provided by the previously reported reaction of tetramethylammonium superoxide with $[(\text{triphos})\text{Rh}(\text{DTBSQ})]^{2+}$ to give the diamagnetic complex $[(\text{triphos})\text{Rh}(\text{OO})(\text{DTBSQ})]^+$ (Scheme 9). In this case, it is reasonable to conclude that the radical O_2^- species pairs its spin interacting with the C(O) atom of the semiquinone ligand to form a peroxo group, which ultimately brings about a nucleophilic attack at the unsaturated metal center.

In light of the reaction of Scheme 9, one might suggest an outer-sphere mechanism involving initial transfer of an electron from the coordinated catecholate to O_2 to give the corresponding semiquinonate species and superoxide, followed by recombination of the semiquinone radical with O_2^- . The argument could be somewhat in agreement with the overall delocalization of the π_{\perp} HOMO of the catecholate that apparently makes a regioselective attack problematic. In any event, a pure outer-sphere mechanism appears unprobable since no $M(\text{III})\text{Cat}/M(\text{III})\text{SQ}$ couple possesses a redox potential capable of reducing O_2 to O_2^- (Table 6).

Ultimately, the idea that the nucleophilic catecholate ligand has a primary role in attracting the O_2 molecule remains most sound although other questions need to be convincingly answered. For example, is the role of the metal atom simply that of accepting, in a donor/acceptor relation, the density accumulated at the free end of the preformed peroxo group or does it also cooperate in promoting the reaction from the early stages? Also, by assuming that the paramagnetic O_2 molecule performs an electrophilic attack, at which point along the pathway does the quenching of its paramagnetism take place?

Since all of the experimental data suggest a strict correlation between the nature of both the catecholate and metal in promoting the formation of the dioxygen



Scheme 9.

adduct, we propose now a mechanism that has the features of a concerted closure of the five-membered metallocycle M–O–C–O–O. The mechanism also recalls that typical of 1,3-cyclo additions in dipolar systems [59]. Even though the two new bonds (C–O and M–O) are likely to form at different rates (probably with a faster C–O formation), the copresence of two poles (negative C(O) and positive metal centers) is the necessary requisite for the reaction to occur via a polarization of the O₂ molecule itself. The latter description finds support in the features of a Walsh diagram (Fig. 10) that monitors the MO evolution for the approach of a free O₂ molecule to a model of the catecholate

precursor (the unique reaction coordinate accounts for the reorientation and deformation of the quinoid ligand found in the structure of the O₂ adduct).

Along the pathway, the levels that are most affected (destabilized) are the former HOMO and LUMO of [(triphos)M(cat)]⁺. This is because the two MOs acquire increasing C–O and Ir–O σ* character, respectively. Most importantly the former HOMO of the precursor is depopulated along the pathway, whereas the deeper two π_g* (O₂) levels, singly populated in the beginning, become eventually, fully saturated. Likely, the electron transfer and the formation of the peroxo group occurs in the early stages of the reaction but O₂ must be

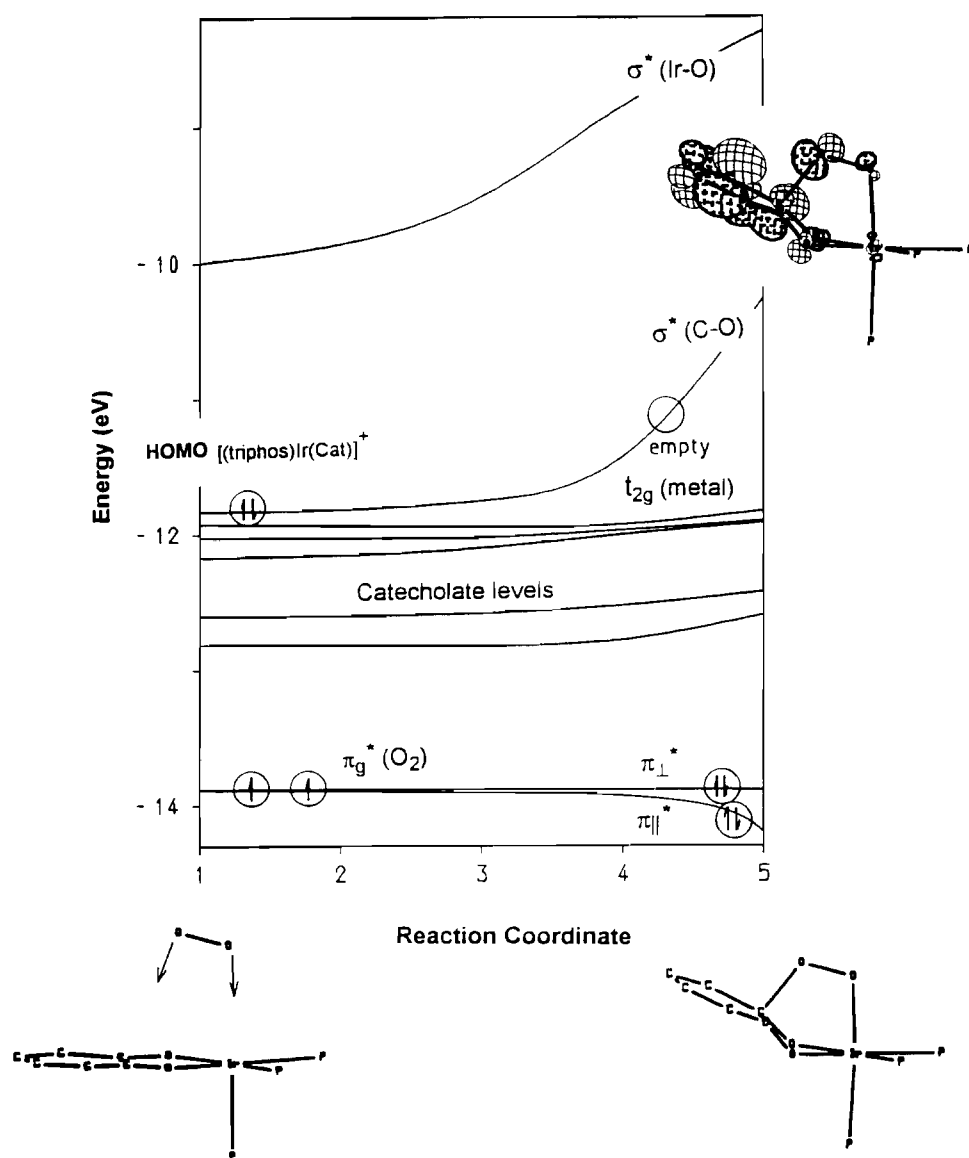


Fig. 10. A Walsh diagram for approaching a O₂ molecule toward [(triphos)Ir(Cat)]⁺. Both the LUMO and the HOMO of the precursor complex are most affected and eventually identify with the σ* components of the newly formed Ir–O and C–O bonds. Notice that the two singly populated π_g* levels of the O₂ molecule are significantly lower than several filled MOs of the complex (some not shown). Early, along the pathway, two electrons are transferred from the complex HOMO (largely catecholate) into O₂ (becoming peroxide).

already interacting with the complex so that it is not correct to define the mechanism as an outer-sphere oxidation. Also, the electron transfer process may be facilitated by the coupling of the two unpaired spins of O₂ in the π_{\perp}^* orbital, but the concertedness of the process excludes that a high energy diamagnetic dioxygen molecule may have a finite lifetime during the process.

In conclusion, the features of the Walsh diagram of Fig. 10 provide a fairly good qualitative idea of what may happen during the reaction. Both the catecholate and the metal centers have an active role from the early stages. There is no evidence whatsoever that, at any point, intermediates are formed in which O₂ is preferentially linked either to the metal or to the catecholate ligand. Basically the metal complex seems to active O₂ because it bears in close proximity an acidic metal and an electron rich (basic) ligand. To state the same concept in MO terms, the bonding capability of the complexes [(triphos)M(cat)]⁺ toward O₂ is largely attributable to the unusual coexistence of a ligand centered HOMO with a metal centered LUMO. As shown in Fig. 10, both levels are almost equally involved in bond formation with O₂ and, on this ground, we suggest that the O₂ activation is made possible by the *bifunctionality* of the metal catecholate complexes.

Supplementary material

Hydrogen atom parameters and observed and calculated structure factor tables are available from the authors on request.

Acknowledgements

Thanks are due to Professor I. Bertini (University of Florence) for helpful discussion and to 'Progetti Finalizzati Chimica Fine e Secondaria II' CNR, Rome, Italy.

References

- 1 C. Bianchini, P. Frediani, F. Laschi, A. Meli, F. Vizza and P. Zanello, *Inorg. Chem.*, **29** (1990) 3402.
- 2 C. Bianchini, D. Masi, C. Mealli, A. Meli, G. Martini, F. Laschi and P. Zanello, *Inorg. Chem.*, **26** (1987) 3683.
- 3 P. Barbaro, C. Bianchini, P. Frediani, A. Meli and F. Vizza, *Inorg. Chem.*, **31** (1992) 1523.
- 4 P. Barbaro, C. Bianchini, C. Mealli and A. Meli, *J. Am. Chem. Soc.*, **113** (1991) 3181.
- 5 (a) L. Jr. Que, *Adv. Inorg. Biochem.*, **5** (1983) 167; (b) L. Jr. Que, *Struct. Bonding (Berlin)*, **40** (1980) 39; (c) T. Funabiki, A. Mizoguchi, T. Sugimoto, S. Tada, M. Tsuji, H. Sakamoto and S. Yoshida, *J. Am. Chem. Soc.*, **108** (1986) 2921; (d) U. Casellato, S. Tamburini, P. A. Vigato, M. Vidali and D. E. Fenton, *Inorg. Chim. Acta*, **84** (1984) 101; (e) M. M. Rogic and T. R. Demmin, *J. Am. Chem. Soc.*, **100** (1978) 5472; (f) S. Tsuruya, S. Yanai and M. Masai, *Inorg. Chem.*, **25** (1986) 141; (g) C. A. Tyson and A. E. Martell, *J. Am. Chem. Soc.*, **94** (1972) 939.
- 6 P. Barbaro, C. Bianchini, A. Meli, M. Peruzzini, A. Vacca and F. Vizza, *Organometallics*, **10** (1991) 2227.
- 7 C. Bianchini, A. Meli, M. Peruzzini, F. Vizza, P. Frediani and J. A. Ramirez, *Organometallics*, **9** (1990) 226.
- 8 C. Bianchini, A. Meli, M. Peruzzini and F. Vizza, *J. Am. Chem. Soc.*, **112** (1990) 6726.
- 9 A. I. Vogel, *A Text Book of Quantitative Inorganic Analysis*, Wiley, New York, 3rd edn., 1961, p. 343.
- 10 N. Walker and D. Stuart, *Acta Crystallogr., Sect. A*, **39** (1983) 158.
- 11 D. T. Cromer and J. T. Waber, *Acta Crystallogr.*, **18** (1965) 104.
- 12 *International Tables of Crystallography*, Vol. 4, Kynoch, Birmingham, UK, 1974.
- 13 G. M. Sheldrick, *SHELX76*, program for crystal structure determinations, University of Cambridge, Cambridge, UK, 1976.
- 14 P. J. Crowley and H. M. Haendler, *Inorg. Chem.*, **1** (1962) 905.
- 15 (a) A. B. P. Lever, P. R. Auburn, E. S. Dodsworth, M. Haga, W. Liu, M. Melnik and W. A. Nevin, *J. Am. Chem. Soc.*, **110** (1988) 8076; (b) C. G. Pierpont and R. M. Buchanan, *Coord. Chem. Rev.*, **38** (1981) 50.
- 16 P. A. Wicklund and D. G. Brown, *Inorg. Chem.*, **15** (1976) 396.
- 17 M. Haga, E. S. Dodsworth and A. B. P. Lever, *Inorg. Chem.*, **25** (1986) 447.
- 18 A. Y. Girgis, Y. S. Sohn and A. L. Balch, *Inorg. Chem.*, **14** (1975) 2327.
- 19 M. E. Cass, N. Rowan Gordon and C. G. Pierpont, *Inorg. Chem.*, **25** (1986) 3962.
- 20 S. R. Sofen, D. C. Ware, S. R. Cooper and K. N. Raymond, *Inorg. Chem.*, **18** (1979) 234.
- 21 M. W. Lynch, M. Valentine and D. N. Hendrickson, *J. Am. Chem. Soc.*, **104** (1982) 6982.
- 22 S. Bhattacharya and C. G. Pierpont, *Inorg. Chem.*, **30** (1991) 2906.
- 23 D. M. Barlex, R. D. W. Kemmitt and G. W. Littlecott, *J. Chem. Soc., Chem. Commun.*, (1971) 199.
- 24 K. D. Magers, C. G. Smith and D. T. Sawyer, *Inorg. Chem.*, **19** (1980) 492.
- 25 W. P. Griffith, C. A. Pumphrey and T. A. Rainey, *J. Chem. Soc., Dalton, Trans.*, (1986) 1125.
- 26 Y. S. Sohn and A. L. Balch, *J. Am. Chem. Soc.*, **94** (1972) 1144.
- 27 J. V. McArdle, S. R. Sofen, S. R. Cooper and K. N. Raymond, *Inorg. Chem.*, **17** (1978) 3075.
- 28 C. Bianchini, A. Meli, M. Peruzzini, F. Vizza, Y. Fujiwara, T. Jintoku and H. J. Taniguchi, *J. Chem. Soc., Chem. Commun.*, (1988) 210.
- 29 C. Bianchini, A. Meli, F. Laschi, F. Vizza and P. Zanello, *Inorg. Chem.*, **28** (1989) 227.
- 30 L. Dahlenburg and F. Mirzaei, *Inorg. Chim. Acta*, **97** (1985) L1.
- 31 S. Harmalker, S. E. Jones and D. T. Sawyer, *Inorg. Chem.*, **22** (1983) 2790.
- 32 S. S. Isied, G. Kuo and K. N. Raymond, *J. Am. Chem. Soc.*, **98** (1976) 1763.

- 33 S. E. Jones, D. H. Chin and D. T. Sawyer, *Inorg. Chem.*, **20** (1981) 4257.
- 34 D. H. Chin, D. T. Sawyer, W. P. Schaefer and J. Simmons, *Inorg. Chem.*, **22** (1983) 752.
- 35 P. Espinet, P. M. Bailey and P. M. Maitlis, *J. Chem. Soc., Dalton Trans.*, (1979) 1542.
- 36 S. R. Sofen, S. R. Cooper and K. N. Raymond, *Inorg. Chem.*, **18** (1979) 1611.
- 37 L. M. Charney, H. O. Finklea and F. A. Schultz, *Inorg. Chem.*, **21** (1982) 549.
- 38 J. P. Wilshire, L. Leon, P. Bosserman and D. T. Sawyer, *J. Am. Chem. Soc.*, **101** (1979) 3379.
- 39 J. R. Hartman, B. M. Foxman and S. R. Cooper, *Inorg. Chem.*, **23** (1984) 1381.
- 40 J. S. Valentine and D. Valentine, *J. Am. Chem. Soc.*, **92** (1970) 5795.
- 41 R. M. Buchanan and C. G. Pierpont, *J. Am. Chem. Soc.*, **102** (1980) 4951.
- 42 P. A. Wicklund, L. S. Beckmann and D. G. Brown, *Inorg. Chem.*, **15** (1976) 1996.
- 43 F. Hartl, A. Jr. Vlcek, L. A. de Learie and C. G. Pierpont, *Inorg. Chem.*, **29** (1990) 1073.
- 44 (a) A. Araneo, F. Morazzoni and T. Napoletano, *J. Chem. Soc., Dalton Trans.*, (1975) 2039; (b) G. Yoneda and D. M. Blake, *J. Organomet. Chem.*, **190** (1980) C71.
- 45 L. A. de Learie, R. C. Haltwanger and C. G. Pierpont, *J. Am. Chem. Soc.*, **111** (1989) 4324.
- 46 S. Bhattacharya, S. R. Boone, G. A. Fox and C. G. Pierpont, *J. Am. Chem. Soc.*, **112** (1990) 1088.
- 47 C. G. Pierpont and R. M. Buchanan, *Inorg. Chem.*, **21** (1982) 652.
- 48 A. Bencini and D. Gatteschi, *Transition Met. Chem.*, **8** (1982) 1.
- 49 (a) C. Bianchini, A. Meli, M. Peruzzini, A. Vacca, F. Laschi, P. Zanello and F. M. Ottaviani, *Organometallics*, **9** (1990) 360; (b) C. Bianchini, *Comments Inorg. Chem.*, **8** (1988) 27; (c) C. Bianchini, F. Laschi, A. Meli, M. Peruzzini, P. Zanello and P. Frediani, *Organometallics*, **7** (1988) 2575; (d) C. Bianchini, F. Laschi, F. M. Ottaviani, M. Peruzzini, P. Zanello and F. Zanolini, *Organometallics*, **8** (1989) 893.
- 50 F. H. Allen, O. Kennard, D. G. Watson, L. Brammer, A. G. Orpen and R. Taylor, *J. Chem. Soc., Perkin Trans. II*, (1987) S1.
- 51 M. Pizzotti, S. Cenini, R. Ugo and F. Demartin, *J. Chem. Soc., Dalton Trans.*, (1991) 65.
- 52 D. D. Cox, S. J. Benkovic, L. M. Bloom, F. C. Bradley, M. J. Nelson, L. Que, Jr. and D. E. Wallick, *J. Am. Chem. Soc.*, **110** (1988) 2026.
- 53 D. D. Cox and L. Que, Jr., *J. Am. Chem. Soc.*, **110** (1988) 8085.
- 54 D. M. Wagnerova, K. Lang and W. Damerau, *Inorg. Chim. Acta*, **162** (1989) 1.
- 55 (a) R. Hoffmann and W. N. Lipscomb, *J. Chem. Phys.*, **36** (1962) 2179; **37** (1962) 2872; (b) R. Hoffmann, *J. Chem. Phys.*, **39** (1963) 1397.
- 56 C. Mealli, to be published.
- 57 (a) M. H. Gubelmann and A. F. Williams, *Struct. Bonding (Berlin)* **55** (1983) 1; (b) H. Mimoun, in G. Wilkinson (ed.), *Comprehensive Coordination Chemistry*, Vol. 6, Pergamon, Oxford, 1987, 318.
- 58 C. Mealli and D. M. Proserpio, *J. Chem. Educ.*, **67** (1990) 399.
- 59 I. Fleming, *Frontier Orbitals and Organic Chemical Reactions*, Wiley-Interscience, London, 1976.